Title: Synthesis and characterization of aluminium-alumina micro- and nano-composites by spark plasma sintering

Author: <ce:author id="aut0005"> K. Dash<ce:author id="aut0010"> D. Chaira<ce:author id="aut0015"> B.C. Ray

PII: S0025-5408(13)00201-8
DOI: http://dx.doi.org/doi:10.1016/j.materresbull.2013.03.014
Reference: MRB 6560

To appear in: *MRB*

Received date: 15-6-2012
Revised date: 4-3-2013
Accepted date: 12-3-2013

Please cite this article as: K. Dash, D. Chaira, B.C. Ray, Synthesis and characterization of aluminium-alumina micro- and nano-composites by spark plasma sintering, *Materials Research Bulletin* (2013), http://dx.doi.org/10.1016/j.materresbull.2013.03.014

Title – Synthesis and characterization of aluminium-alumina micro- and nano-composites by spark plasma sintering

Authors – Khushbu Dash, Debasis Chaira, Bankim Chandra Ray

Author affiliations –

Corresponding author

Khushbu Dash
Research Scholar
Dept. of Metallurgical and Materials Engg.
National Institute of Technology,
Rourkela – 769008
Phone – +91-9439281130(M)
Fax - +91-661-2465999
E-mail – khushbudash@gmail.com

Co-authors

Debasis Chaira
Asst. Professor
Dept. of Metallurgical and Materials Engg.
National Institute of Technology,
Rourkela – 769008
Phone – +91-661-2462561(O)
Fax - +91-661-2465999
E-mail – chaira.debasis@gmail.com

Bankim Chandra Ray
Professor
Dept. of Metallurgical and Materials Engg.
National Institute of Technology,
Rourkela – 769008
Phone – +91-9437221560 (M)
Fax - +91-661-2465999
E-mail – drbcray@gmail.com

Synthesis and characterization of aluminium-alumina micro- and nano-composites by spark plasma sintering

K. Dash*[a], D. Chaira[a] and B.C. Ray[a]

[a]Department of Metallurgical & Materials Engineering

National Institute of Technology Rourkela, Rourkela – 769008, India

Corresponding author: Khushbu Dash

Address: Dept. of Metallurgical and Materials Engineering., National Institute of Technology, Rourkela – 769008

E-mail: khushbudash@gmail.com

Phone no: +91 661 2640369

Fax - +91-661-2465999

Abstract

In the present study, an emphasis has been laid on evaluation of the microstructural morphologies and their implications on mechanical performance of the composites by varying the reinforcement particle size. Nanocomposites of 0.5, 1, 3, 5, 7 volume % alumina (average size<50nm) and microcomposites of 1, 5, 20 volume % of alumina (average size~10μm) reinforced in aluminium matrix were fabricated by spark plasma sintering technique at a temperature of 773K and pressure of 50 MPa. These micro- and nano-composites have been characterized using X-ray diffraction, scanning electron microscopy and transmission electron microscopy followed by density, microhardness and nanoindentation hardness measurements.

The alumina nanoparticles revealed appreciable physical intimacy with the aluminum matrix than that of alumina microparticles. The highest nanohardness recorded 0.85 GPa and 99% densification for 7 and 1 vol. % Al-Al_2O_3 nancomposites respectively. Spark plasma sintering imparts enhanced densification and matrix-reinforcement proximity which have been corroborated with the experimental results.

Keywords: A. Composites; C. Electron microscopy; D. Microstructure.

1. Introduction

Composites have conferred revolutionary materials around the globe for structural, mechanical, automobile as well as other critical applications where the property value needs to be tailored. The physical and mechanical superiority of nano-structured materials has fascinated scientists in recent times [1]. The strengthening due to grain refinement can be delegated to a number of theories such as the Hall-Petch relation, Orowan bowing mechanism, Taylor relationship and several other models [2]. Aluminum is a potent material for aerospace as well as military and electronics applications because it possesses high specific strength, high toughness and corrosion resistance [3]. Aluminium poses poor wear resistance which can be improved by the addition of ceramic reinforcements.

In general, there are two processing routes to incorporate ceramic particulates into aluminium. Introduction of ceramic particulates into the matrices via ingot casting and powder metallurgy (PM) processes are most popular [4]. Another classification of processing aluminium matrix composites is ex-situ and in-situ methods of fabrication. In ‘ex-situ’ MMCs the ceramic particulates are synthesized separately prior to the composite fabrication, which often results in

agglomeration of fine ceramic particulates during processing. The in-situ route provides several advantages over conventional ex situ process, e.g. in situ formed reinforcements are more uniformly distributed, finer in size, and thermodynamically stable leading to superior mechanical properties compared to their ex situ counterparts [5]. The powder metallurgy route in case of oxide reinforcements has an added advantage as they follow the energy efficient method [6]. The greatest threat in this fabrication route is the absence of an integrated interface formation as the metal powders are less reactive in solid state [7].

The conventional method of sintering renders coarse microstructure, poor adhesion and density, low strength and hardness at high temperatures. There is a need of advanced sintering techniques to obtain finer microstructures. The spark plasma sintering technique is becoming popular due to intrinsic advantages of the method, enhanced material properties, as well as lower processing temperature and shorter sintering time to consolidate powders compared to conventional methods. Spark plasma sintering (SPS) is a novel method for consolidating nanocrystalline materials with stunted grain growth, effective shrinkage in less time as well as cleaner grain boundaries for effective interface formation [8]. Spark plasma sintering is an excellent method for sintering nanomaterials as well as micromaterials because of its unique features such as high heating rates, shorter processing time as well as effective bonding between particles. SPS has the advantage of combining the effects of axial mechanical loading, temperature and electric current. The current plays two roles in SPS i.e. current is the source of heating by Joule effect and promotes enhanced diffusion rate during phase growth and intermetallic diffusion [9]. The advent of nanostructured material production techniques have led to an unprecedented growth in the area of metal matrix composites with extraordinary superior strengths. The strengthening

mechanisms of metal matrix composites include the grain size effect and the generation of geometrically necessary dislocations [10]. The surplus strength entitled to the material has to be compromised with the loss in ductility. The strength-ductility dichotomy can be alleviated by using small volume fraction of inclusions (reinforcements). Alumina is a strength boon to the matrix because it is chemically stable, inert and non reactive at high temperatures. Degree of dispersion of reinforcement particles in the matrix is an essential parameter to determine the mechanical performance index of a particulate reinforced composite.

The zone between the matrix and reinforcement phase (interface or interphase) is an essential part of MMC. Bonding between the two phases develops from interfacial frictional stress, physical and chemical interaction and thermal stresses due to mismatch between coefficient of thermal expansion of matrix and reinforcement. During the designing of a MMC the underlying interfacial phenomenon governing the transmission of thermal, electrical and mechanical properties is of utmost importance [7]. The physicochemistry of wetting and bonding of oxide reinforcements with the metal matrix (i.e. the non reactivity at the interface zone) in terms of Gibbs free energy change ΔG^{O}_{r} is as follows

$$n\,Me + m\,MO_n = n\,MeO_m + m\,M \qquad (1)$$

where Me is the matrix and MO_n is the reinforcing oxide. The Gibbs free energy is strongly positive in this case; therefore it has been proposed that the oxide reinforcements can have only Vander Waals kind of interaction with metal matrices arising from dispersion forces. Some groups [11-14] who were working on the thermodynamic aspects of wetting of metal/oxide couples have reported large variations between the experimental results and the theoretical

considerations. The work of adhesion W_a plays a major role in determining the level of interaction of matrix and reinforcement. The more the W_a the better the adhesion [15].

The interfacial failure needs to be evaluated accurately to estimate the performance of a metal matrix composite. The interfacial failure in case of particulate reinforced metal matrix composite has not been apprehended comprehensively till date. Several groups [16-19] have reported the basic mechanisms of interfacial failure in particle reinforced metal matrix composites as interface decohesion, damage accumulation, solute segregation, thermal misfit dislocation density, reinforcement geometry and clustering. To quantify the interfacial failure we need to understand the sintering response in context to the matrix-reinforcement alliance and the later depends directly on the reinforcement particle size and PSR (particle size ratio). Razavi Hesabi et al. [20] studied the compressibility of aluminium/nanometric alumina and have drawn a comparison between blended and milled powders. Rahimian et al. [21] have investigated that proper sintering parameters result in improved wear properties of Al-Al_2O_3 composites. Gudlur et al. [22] studied the variation in porosity with particle size and predicted their mechanical and thermal properties in Al-Al_2O_3 system. Tatar et al. [23] have reported the improvement of thermal conductivity of Al-Al_2O_3 composites with different alumina content. Many other groups have studied the microstructural and mechanical aspects of Al-Al_2O_3 system. The sinterability, microstructural variations, interfacial compatibility and integrity correlated with the variation in micro- and nano-reinforcement sizes fabricated with the aid of spark plasma sintering has not been discussed till date.

The present study focuses on the fabrication of Al-Al_2O_3 nanocomposites and microcomposites by spark plasma sintering technique. The microstructural study of different vol. % (0.5, 1, 3, 5, 7) alumina nanoparticles and 1, 5, 20 vol. % alumina microparticles reinforced aluminium matrix composites has been conducted with the help of scanning electron microscopy and transmission electron microscopy. The microstructural investigation gives an insight into the interaction of matrix and reinforcement particles, the dispersion of the reinforcements in the matrix as well as porosity. The properties like density, microhardness and nanoindentation hardness have been measured to evaluate the level of engineering performance. The variation in particle size of reinforcement particle leads to a series of events (all of which have not been understood properly) starting from blending to sintering. The correlation of interface formation, bonding and matrix microstructure with the size of reinforcement needs a detailed study and the present work is an actualization towards it. The Al-Al_2O_3 micro- and nano-composites have been fabricated using spark plasma sintering. The comparison of Al-Al_2O_3 micro- and nano-composites in terms of microstructural evolution and mechanical properties have been emphasized here. The benefit of spark plasma sintering in retaining nanostructure during high temperature sintering and effect of spark plasma sintering on the processing of Al-Al_2O_3 micro- and nano-composites has been investigated in this study.

2. Experimental

The as-received aluminium (Loba Chemie, purity > 99.7%, average size~22.09μm) and alumina (Sigma Aldrich, average size~10μm and <50 nm) (surface area: 40 m^2/g for alumina nanopowder) powders were mixed and blended separately using agate mortar for 60 minutes to ensure homogeneous mixing. The phase analysis and microstructure of as received alumina micro and nanopowders have been carried out. Nanocomposites containing 0.5, 1, 3, 5 and 7 vol.

% of Al_2O_3 (average size<50nm) were fabricated by blending the matrix and reinforcement powders, followed by spark plasma sintering (SPS) (DR SINTER LAB SPS Syntex). Another set of specimens having compositions of 1, 5, 20 volume% were chosen to fabricate microcomposites. SPS was carried out at a temperature of 773 K and an applied pressure of 50MPa for 5 minutes under vacuum with a heating rate of 353 K/minute for nanocomposites as well as the microcomposites. The as-received aluminium and alumina powders were characterized by particle size analyzer (MALVERN Mastersizer 2000) BET surface area analyser (Quantachrome Autosorb) while sintered specimens were characterized by X-Ray diffractometer (PANalytical model: DY-1656) using $Cu_{K\alpha}$ radiation, scanning electron microscopy (JEOL 6480 LV) and transmission electron microscopy (FEI Tecnai G2 20 S-TWIN). The specimens were prepared by chemically etching with Keller's reagent for metallographic study. The sample preparation for TEM was performed by initially reducing the thickness below 100µm and then making a 3 mm disc by mechanical punching. The discs were then dimpled to around below 10µm and then ion milled for 1 hour for perforation.

The density values were recorded using Archimedes water immersion method. The micro-hardness values of all the specimens were determined by Vickers hardness tester (Leco LV 700) applying a load of 0.3 kgf and a dwell time of 5 seconds. The readings were recorded here at four equivalent locations for each specimen. The nanoindentation hardness values were determined using nanoindentation (Fisher-Cripps UMIS) technique applying a load of 20mN for a dwell time of 10 seconds. The readings were recorded here at ten equivalent locations for each specimen and the closest values were considered.

3. Results and Discussion

3.1. X-ray diffraction

The X-Ray diffraction patterns obtained from the SPS sintered compacts of the Al-Al_2O_3 nanocomposites reveal aluminium as well as alumina phases. The X-Ray diffraction patterns of the Al-Al_2O_3 microcomposites and nanocomposites are shown in Fig. 1(a) & (b) respectively. The patterns depict small peaks of alumina present in the X-Ray patterns of nanocomposites (the combined effect of peak broadening and low intensity peaks of alumina nanoparticles visible in Fig. 1(c)) whereas in case of microcomposites, the alumina peaks are quite distinct and clear. The XRD patterns of as-received alumina micro- and namo-powders have been illustrated in Fig. 1(c) & (d). The patterns show distinct difference in terms of peak broadening and hence particle size and phases. The XRD patterns confirm that no new phase was formed in the nano- and microcomposites. The alumina peaks are distinct in the 20 vol. % reinforced Al-Al_2O_3 microcomposite due to higher amount of alumina.

3.2. Scanning electron microscopy

The micrographs of as received alumina micro- and nano-particles have been illustrated in Fig. 2(a) & (b). Fig. 2(a) shows that the shape of alumina particles is acicular and Fig. 2(b) shows dispersed regions as well as agglomeration of nanoparticles. The back scattered scanning electron micrographs of Al-Al_2O_3 nanocomposites are illustrated in Fig. 2(c), (d) & (e) indicating grey and black regions which correspond to the aluminum and alumina respectively confirmed by EDS analysis. Fig. 2(d) shows the EDS analysis of the black region in the figure depicted by arrow mark. The alumina nanoparticles are present in the interspaces of aluminium particles. The

distribution of reinforcement particles in Al-Al_2O_3 nanocomposites is proficient than in the case of microcomposites. The well established mathematical relation (Eq. (2)) which explains the requirement of uniform dispersion of reinforcement in the matrix

$$\lambda = \frac{4(1-f)r}{3f} \qquad (2)$$

Where λ is distance apart from the reinforcements, f is the fractional volume of reinforcement; r is the radius of the particles (assuming them to be spherical). The SEM micrographs of the nancomposites suggest presence of network of the alumina particles within the intergranular spaces of the aluminium matrix. The micrographs connote the intimate level of mixing of matrix and reinforcement powders in the nanocomposites which is seemingly due to the aluminium-alumina bonding in the composite. The proximate level of intermixing of alumina nanoparticles in the aluminium matrix has supposedly given rise to such a microstructure. A striking difference regarding the mode of interaction of alumina nanoparticle and alumina microparticle with the aluminium matrix individually can be realized from the micrographs. The differential interaction of nanoparticles and microparticles could be implicated to the reason of clustering in composites, the closer the ratio of reinforcement particle size to the matrix particle size (PSR) is to 1 the lower is the possibility of clustering [24]. The clustering which is apparently visible in the case of microcomposite is due to the deviation of the ratio from the value 1.

In nanocomposites, the reinforcement particle size is much smaller than the matrix particle size, and hence the inter-particle voids created by the consolidation of aluminium particles have been occupied by the alumina nanoparticles. The conspicuous bonding of nanoparticles with the matrix particles can also be due to the fact that the atomic diffusivity of the nanoparticles is quite high than the micron-sized particles [25]. The micron-sized alumina particles are quite large in

size when compared to the matrix particles, so they have created an extra space to get accommodated into the matrix. Whereas the accommodation of alumina nanoparticles is better in the aluminium matrix i.e. the alumina nanoparticles have occupied the interparticle spaces in the aluminium matrix which is not the case with microcomposites. The grain growth in the microcomposites is likely to occur to a greater extent than in nanocomposites. This observation could be attributed to the inability of the alumina microparticles to pin down the grain growth at a larger scale. The thermal stability against grain growth observed in the nanocomposites can be ascribed to the presence of alumina nanoparticles which are expected to hinder the grain boundary movement via Zener pinning [26].

Incipient fusion phenomenon probably has occured which can be observed in the nanocomposites in between the intergranular spaces of aluminium, which can be ascribed to plasma formation at interparticle contacts at the time of sintering. The pores present in the nanocomposites are sparse in number which can be observed in SEM micrograph i.e. Fig. 2(c), (d) & (e) as compared to the microcomposites shown in Fig. 3(a), (b) & (c). The poor bonding of aluminium and alumina nanoparticles has been reported in literature by conventional sintering [27]. The distribution of alumina in nanocomposites is better than in the microcomposites which have been illustrated in Fig. 3(a), (b) & (c). The improved bonding between the matrix and reinforcement by spark plasma sintering method can be attributed to the pressure assisted sintering as well as the grain boundaries rendered clean in the process of SPS.

Olevsky et al. [28] have investigated the impact of thermal diffusion in spark plasma sintering which reflects that the non-uniform distribution of temperature causes local melting at the interparticle contacts. Munir et al. [8] have demonstrated higher diffusion co-efficient for spark plasma sintering. Xie et al. [29] have studied the spark plasma sintering of aluminium powders

and have reported the presence of a clean interface from high resolution TEM experiments. In the present investigation, clean interface (absence of interphase or reaction products) and a reasonable amount of physical contact of the alumina particles to the aluminum particles has also been observed. The dispersion of reinforcements in the matrix is the blue print of the degree of strengthening rendered by the reinforcement particles.

3.3. Transmission electron microscopy

The transmission electron microscope (TEM) micrographs illustrate the dispersion of alumina particles in aluminium matrix. The grey region symbolizes aluminium matrix and the black area depict alumina particles which have been confirmed by EDAX analysis. The TEM micrographs of the sintered specimen show clean and sound interface in case of both nano- and microcomposites [30]. The alumina particle size can be estimated to be around 50 nm from the TEM micrograph in Fig. 4(a), (b) & (c). In Fig. 4(a) Frank fault loops (marked by black arrows) can be observed inside the alumina particles [31]. These loops impart a conviction of the strengthening mechanisms operating in the composite [32]. The SAD pattern of the Al-5% reinforced Al_2O_3 nanocomposite has been illustrated in Fig. 4(b). The SAD pattern shows mainly ring patterns along with some spots are present confirming the existence of nanoparticles.

Fig. 5(a) shows large numbers of dislocations are accumulated at the triple junction of Al-7% reinforced Al_2O_3 nanocomposite. It can also be observed that the dislocations are pinned and piled up at the Al/Al_2O_3 interface. Fig. 5(b) illustrates the presence of screw dislocations in Al-Al_2O_3 microcomposites. The dislocation lines are straight, long and tangled indicating high dislocation density, which probably arises during spark plasma sintering process. During SPS the powder mass has undergone heavy deformation due to simultaneous application of pressure and

high temperature. Pure tilt boundaries are visible in Fig. 5(c) [33]. The deformed FCC crystals when annealed lead to interactions between 1/2<*110*> dislocations resulting in the formation of low-energy networks and sub-boundaries. This refers to: when dislocations' motion is impeded from moving in their slip plane by interacting with other dislocations, sub- boundaries, and others, the strain energy can be minimized by the dislocations climbing out of slip planes where they align in low energy configurations, e:g: cell walls. The high dislocation density at the sub-boundaries can be attributed to the large difference in thermal conductivity of aluminium (24 x 10^{-6}/°C) and alumina (7.92 x 10^{-6}/°C). Cooling of the composite furnishes limited deformation of aluminium inhibited by alumina particles, hence high dislocation density at the boundaries [34].

Fig. 5(d) shows a stacking fault [31] present in the microcomposite, which could be explained as follows: the intermixing of alumina microparticles in the matrix is inappreciable; therefore there may be formation of some sessile dislocations during packing of matrix and microparticle powders. As dislocation is a temperature driven phenomenon, the sessile dislocations formed must have resulted in stacking fault at the time of sintering [32]. During sintering, the energy supplied by the combined elasto-plastic (compression) and electro-magnetic (discharge) processes imparts sufficient mobility for movement of edge dislocations [35]. A sessile dislocation can move only by the diffusion of atoms or vacancies to or from the fault. The width of the stacking fault ribbon is directly proportional to the stacking fault energy which is quite prevalent in case of aluminium.

3.4. Density measurement

The density measurements exhibit close values to % of theoretical density for microcomposites and nanocomposites (Table 1). The microcomposites exhibit poor bonding and compatibility of alumina in the aluminium matrix. The % of theoretical density of microcomposites and nanocomposites falls as the volume of alumina increases. The density values of 5% alumina reinforced microcomposite are higher than the corresponding nanocomposite density values. The underlying reason could be that compressibility of hard nanoparticles in a ductile matrix is tedious. The compressibility of hard and non-deformable particles in a ductile matrix decreases with increasing content of the hard particles (reinforcements) [36]. Moreover the formation of networks also retards compaction. This is the same reason for which the density plot shows a steep fall from 1 to 5 vol. % of alumina.

The density data for nanocomposites are scattered but the trend of density values with increasing amount of reinforcement is negative. This can be attributed to the plastic deformation of aluminium particles through particle contact during compaction. The higher alumina content increases alumina-alumina contact which impedes the deformability of aluminium particles [37]. Hence, the densification trend shows a downfall with the increase in alumina content. The major concern of nanoparticles is agglomeration as well as the tendency to form interconnected networks. The problem of agglomeration in nanoparticles leads to lesser densification in nanocomposites whereas this does not impair the densification of microcomposites to a larger extent. This is due to the fact that the specific surface of coarser particles is lower and the powder compressibility is higher [38]. Rahimian et al. [26] have obtained 96.8% of relative

density for Al-10wt% Al_2O_3 conventionally sintered at 500˚C where as we have reported 98.8% for Al-1%Al_2O_3 microcomposite and 99.5% relative density for Al-1%Al_2O_3 nanocomposite.

3.5. Microhardness and nanohardness measurements

The microhardness measurements show high hardness values for nanocomposites than for microcomposites which are visible in Table 1. In case of nanocomposites hardness increases upto 5 vol. % of alumina due to the positive effect of dispersion strengthening but after that it decreases due to agglomeration of nanoparticles. The micron sized particles have lower tendency to agglomerate compared to nanoparticles hence, it is attributed to the effect of positive dispersion strengthening. The micron-sized particles were inefficient to pin down the grain growth of the aluminium grains compared to the alumina nanoparticles. Agglomeration of nanoparticles results in the increase of interparticle distance subsequently reducing the particle-dislocation interaction. Moreover less strength is required to move a dislocation where the interparticle distance is large. The nanoparticles possess high yield stress, sensitive to work hardening so render lesser compressibility. Hence, nanocomposites possess higher microhardness (for 5 vol. %) referring to greater hardening response [37]. The grain growth stagnation in nanocomposites occurs due to Zener effect [39]. Solute segregation is another method for grain growth stagnation. Since the alumina particles are hard and in nanoscale range, high energy is required for the movement of dislocations when they encounter a hard nanoparticle (Dieter, 1976).

$$\tau_0 = \frac{Gb}{\lambda} \qquad (3)$$

where τ_0 is the stress required for a dislocation to pass reinforcement, G is the shear modulus of the material and b is the burger vector of the dislocation. It is very difficult to make exact comparison of microstructure and mechanical properties of composites fabricated by conventional sintering and present SPS method as the processing parameters and raw materials sizes are different. However, we have achieved higher hardness at lower processing temperature and time as compared to conventional sintering [26].

The nanohardness values of the nanocomposites are higher than the corresponding microhardness values (Table 1). This could be attributed to the indentation size effect explained by Mukhopadhyay and Paufler [40]. In microhardness measurements the hardness values of microcomposites (for 5 vol. % of alumina) is lower than that of nanocomposites. The enhanced strength of the nanocomposites can be attributed to the stronger diffusional bonds and structural integrity achieved due to greater diffusional activity [41] by sintering the alumina nanoparticles and aluminium matrix particles by spark plasma sintering. The highest value of microhardness is revealed by the 20 vol. % alumina reinforced microcomposite. The highest amount of alumina could be the reason for the highest value of microhardness.

4. Conclusions

Al-Al_2O_3 nanocomposites with 0.5, 1, 3, 5, 7 vol. % alumina nanoparticles and microcomposites with 1, 5, 20 vol. % alumina micron size particles were fabricated successfully by spark plasma sintering method. The distribution of alumina particles in the aluminium matrix is homogeneous and uniform both in nanocomposites and microcomposites (slightly better distribution in nanocomposites than microcomposite). The interface of aluminium and alumina in nanocomposites is seemingly sound than in the case of microcomposite i.e. the compatibility of

alumina in aluminum matrix in nanocomposites is better than in the microcomposites. The TEM and SEM micrographs reveal a lack of intimate proximity between matrix and reinforcement entities in microcomposites. Almost full densification in case of 1 vol. % alumina reinforced nano- and microcomposites have been achieved. The density of microcomposites as well as nanocomposites decreases with increasing alumina content. The nanohardness of nanocomposites is higher than the corresponding microhardness values. The highest nanohardness recorded was 0.85 GPa for 7 vol. % Al-Al_2O_3 nancomposites.

The significant advances in the present work have been enlisted as follows:

1. The synthesis and characterization of spark plasma sintered Al-Al_2O_3 micro- and nano-composites have been reported in this work. The evolution of microstructures, density, micro- and nano-hardness of micro- and nano-composites has been investigated and compared in the present study.
2. The method of synthesis followed was powder metallurgy route, consolidation by spark plasma sintering technique.
3. The characterization techniques used were X-ray diffraction, scanning electron microscopy, transmission electron microscopy, microhardness tester and nano-indentation hardness measurement technique.
4. The matrix-reinforcement physical integrity is better in nanocomposites than microcomposites as observed from SEM micrographs. Almost full densification (99% of theoretical density) was achieved for nanocomposites and nano-indentation hardness of 0.85 GPa for 7 vol. % alumina reinforced nanocomposite. High density and hardness values for nanocomposites than microcomposites. High dislocation density and

dislocation network at the matrix-reinforcement interface in spark plasma sintered composites.

Acknowledgments

The authors would like to thank the National Institute of Technology (NIT), Rourkela for providing the necessary financial and infrastructural supports. The authors are also grateful to Prof. Bikramjit Basu, Laboratory of Biomaterials, Indian Institute of Technology, Kanpur for coordinating in the preparation of samples using Spark Plasma Sintering facility. The authors also express their gratitude to IMMT, Bhubaneswar for nanoindentation measurements.

References

[1] S. Choi, H. Awaji, Sci. Technol. Adv. Mater. 6 (2005) 2-10.

[2] Y. Li, Y.H. Zhao, V. Ortalan, W. Liu, Z.H. Zhang, R.G. Vogt, N.D. Browning, E.J. Lavernia, J.M. Schoenung, Mat. Sci. Eng. A. 527 (2009) 305-316.

[3] S. Lim, T. Imai, Y. Nishida, T. Choh, Scripta. Mater. 32 (1995) 1713-1717.

[4] S.C. Tjong, Z.Y. Ma, Mat. Sci. Eng. 29 (2000) 49-113.

[5] Y. Peng, M. Zhi, S.C. Tjong, Mater. Chem. Phys. 93 (2005) 109–116.

[6] R. German, Powder Metallurgy, second ed., John Wiley and Sons, Inc, New York, 1994.

[7] S. Vaucher, O. Beffort: MMC-Assess Thematic Network, EMPA-Thun, 9.

[8] Z.A. Munir, Dat V. Quach, J. Am. Ceram. Soc. 94 (2011) 1–19.

[9] N. Chennoufi, G. Majkic, Y.C. Chen, K. Salama, Metall. Mater. Trans. A. 40A (2009) 2401-2409.

[10] R.W. Hertzberg, Deformation and fracture mechanics of engineering materials, fourth ed., John Wiley and sons., 1996.

[11] C.A. Handwerker, J.W. Cahn, J.R. Manning, Mat. Sci. Eng. A. 126 (1990) 173-189.

[12] A. Koltsov, F. Hodaj, N. Eustathopoulos, J. Eur. Ceram. Soc. 29 (2009) 145-154.

[13] P. Hicter, D. Chatain, A. Pasturel, N. Eustathopolous, J. de Chim Phys. 85 (1988) 941-945.

[14] D. Chatain, I. Rivollet, N. Eustathopolous, J. de Chim Phys. 83 (1986) 561-567.

[15] S. Suresh, A. Mortensen, A. Needleman, Fundamentals of metal matrix composites, Butterworth –Heinemann, Stoneham., 1993.

[16] G.G. Sozhamannan, S. BalasivanandhaPrabu, R. Paskaramoorthy, Mater. Des. 31 (2010) 3785–3790.

[17] X.J. Wang, K. Wu, W.X. Huang, H.F .Zhang, M.Y. Zheng, D.L. Peng, Compos. Sci. Technol. 67 (2007) 2253–2260.

[18] M. Gupta and M.K. Surappa, S. Qin, J. Mater. Process. Technol. 67 (1997) 94-99.

[19] G. Liu, Z. Zitang , J. K. Shang, Acta metal. mater. 42 (1994) 271-282.

[20] Z. Razavi Hesabi, H.R. Hafizpour, A. Simchi, Mat. Sci. Eng. A454 (2007) 89–98.

[21] M. Rahimian, N. Parvin, N. Ehsani, Mater. Des. 32 (2011) 1031–1038.

[22] P. Gudlur, A. Forness, J. Lentz, M. Radovic, A. Muliana, Mat. Sci. Eng. A. 531 (2012) 18-27.

[23] C. Tatar, N. Ozdemir, Physica B. 405 (2010) 896–899.

[24] A. Kelly, C. Zweben: Comprehensive composite materials, first ed., Elsevier Science Ltd., 2000 pp.139-149.

[25] G. S. Upadhyaya, Sci. Sinter. 43 (2011) 3-8.

[26] M. Rahimian, N. Parvin, N. Ehsani, Hamid reza Baharvandi, J. Mater. Process. Technol. 209 (2009) 5387-5393.

[27] M. Rahimian, N. Parvin, N. Ehsani, Mat. Sci. Eng. A. 527 (2010) 1031-1038.

[28] E.A. Olevsky, L. Froyen, J. Am. Ceram. Soc. 92 (2009) 122-132.

[29] G. Xie, O. Ohashi, M. Song, K. Furuya, J. Noda, Mett Trans A. 34A (2003) 699-703.

[30] T.G. Durai, K. Das, S. Das, Mat. Sci. Eng. A. 445 (2007) 100–105.

[31] J.W. Edington, Interpretation of transmission electron micrographs, Macmillan., London, 1975.

[32] George E. Dieter, Mechanical Metallurgy, third ed., McGraw-Hill Book Co., New York, NY, 1988.

[33] T. Zhang, Q. Meng, Y. Wang, Y. Zhou, G. Song, J. Mater. Process. Tech. 27 (2011) 553-558.

[34] H. Wang, G. Li, Y. Zhao, G. Chen, Mat. Sci. Eng. A. 527 (2010) 2881-2885.

[35] A. Fais, M. Leoni, P. Scardi, Metall. Mater. Trans. A. 2 (2011) 1-5.

[36] C.A. Leon, G. Rodriguez-Ortiz, E.A. Aguilar-Reyes, Mat. Sci. Eng. A. 526 (2009) 106-112.

[37] S.S. Razavi-tousi, R. Yazdani-Rad, S.A. Manafi, Mat. Sci. Eng. A. 528 (2011) 1105-1110.

[38] D. Roy, A. Sinha, P.P. Chattopadhyay, I. Manna, Mat. Sci. Eng. A. 528 (2011) 8047-8050.

[39] Z. Razavi Hesabi, A. Simchi, S.M. Seyed Reihani, Mat. Sci. Eng. A. 428 (2006) 159-168.

[40] N.K. Mukhopadhyay, P. Paufler, Int. Mater. Rev. 51 (2006) 209-245.

[41] S.K. Karak, J. Dutta Majumdar, W. Lojkowski, A. Michalski, L. Ciupinski, K.J. Kurzydłowski, I. Manna, Philos. Mag. 92 (2012) 516-534.

Figure captions

Fig. 1: XRD diffraction patterns of (a) Al-Al_2O_3 microcomposites (b) Al-Al_2O_3 nanocomposites sintered using SPS (c) as-received alumina micropowder and (d) as-received alumina nanopowder.

Fig. 2: SEM micrographs of (a) as-received alumina micropowder (b) as-received alumina nanopowder (c) Al-1vol. % Al_2O_3, (d) Al-5vol. % Al_2O_3, (e) Al-7vol. % Al_2O_3 nanocomposites sintered using SPS.

Fig. 3: SEM micrographs of (a) Al-1vol. % Al_2O_3, (b) Al-5vol. % Al_2O_3 and (c) Al-20vol. % Al_2O_3 microcomposites sintered by SPS.

Fig. 4: TEM micrographs of (a) Al-1vol. % Al_2O_3, (b) Al-5vol. % Al_2O_3 and (c) Al-7vol. % Al_2O_3 nanocomposites sintered by SPS.

Fig. 5: TEM micrograph of (a) Al-7vol. % Al_2O_3 nanocomposite, (b) (c) & (d) Al-5vol. % Al_2O_3 microcomposite sintered by SPS.

Table captions

Table 1: Density, microhardness and nanoindentation hardness values of Al-Al_2O_3 micro- and nano-composites

Graphical Abstract

The evolution of microstructure by varying the particle size of reinforcement in the matrix employing spark plasma sintering has been demonstrated here in Al-Al_2O_3 system. An emphasis has been laid on varying the reinforcement particle size and evaluating the microstructural morphologies and their implications on mechanical performance of the composites. Nanocomposites of 0.5, 1, 3, 5, 7 volume % alumina (average size<50nm) reinforced in aluminium matrix were fabricated by powder metallurgy route using spark plasma sintering technique technique at a temperature of 773K and pressure of 50 MPa. Another set of specimens having composition 1, 5, 20 vol. % of alumina (average size~10μm) had been fabricated to compare the physical as well as mechanical attributes of the microcomposite as well as the nanocomposites. These micro- and nano-composites have been characterized using X-ray diffraction, scanning electron microscopy and transmission electron microscopy followed by density, microhardness and nanoindentation measurements. The alumina nanoparticles revealed an interface showing appreciable physical intimacy with the aluminum matrix compared to that of the alumina microparticles. The interfacial integrity in case of nanocomposites is better than in the microcomposite which has been studied using microscopic techniques. Spark plasma sintering imparts enhanced densification as well as matrix-reinforcement proximity which has been corroborated with the experimental results.

Keywords: A. Composites; C. Electron microscopy; D. Microstructure

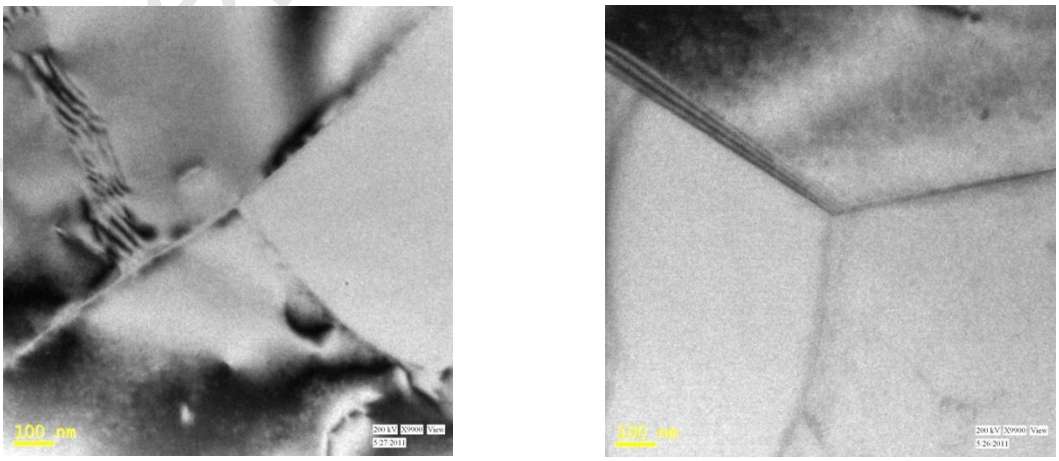

TEM micrograph of Al-7vol. % Al_2O_3 nanocomposite (right) and Al-5vol. % Al_2O_3 microcomposite (left).

Research Highlights

- The Al-Al_2O_3 micro- and nano-composites fabricated by spark plasma sintering.
- Better matrix-reinforcement integrity in nanocomposites than microcomposites.
- Spark plasma sintering method results in higher density and hardness values.
- High density and hardness values of nanocomposites than microcomposites.
- High dislocation density in spark plasma sintered Al-Al_2O_3 composites.

Figure(s)

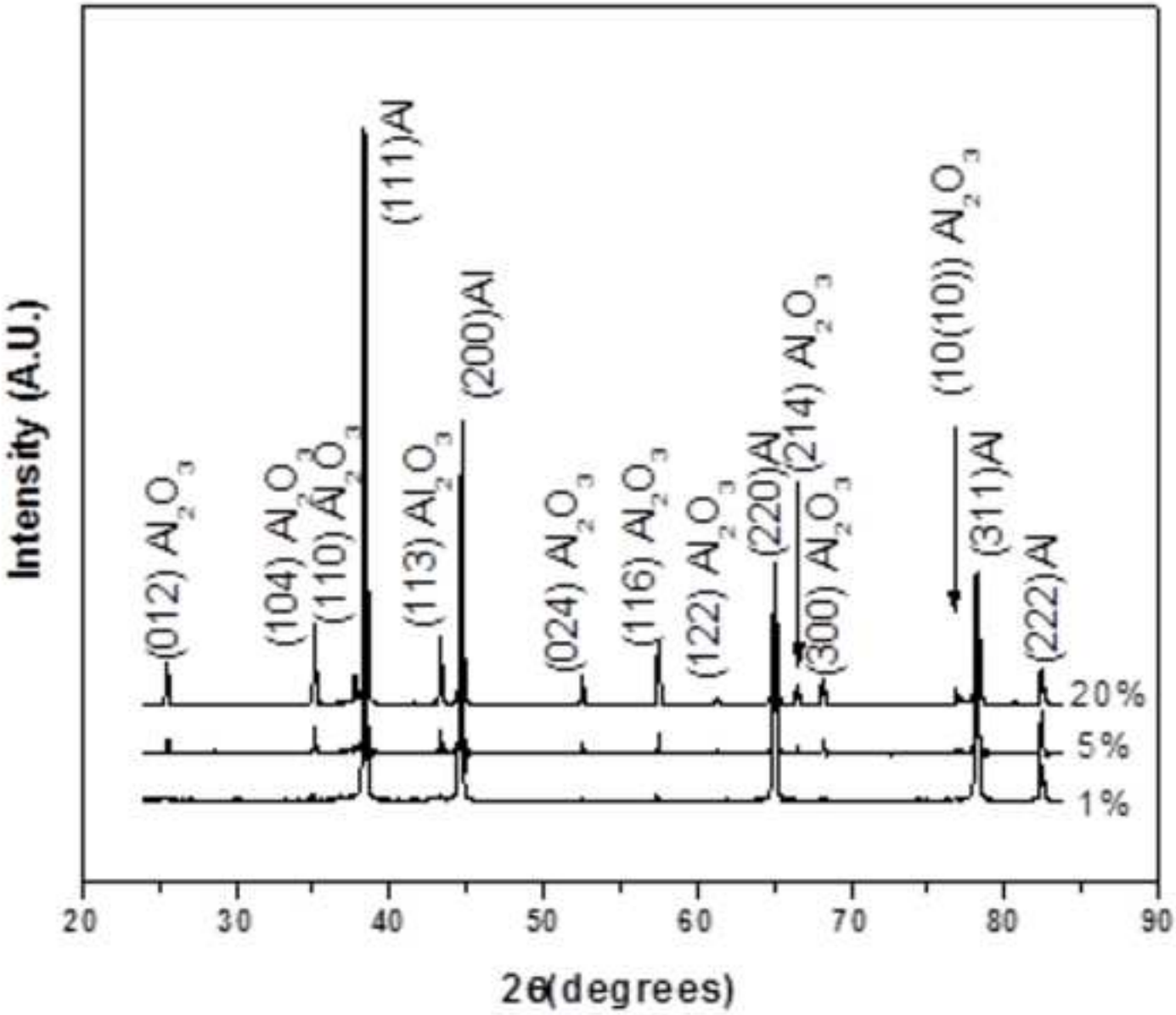
Intensity (A.U.)
2θ(degrees)
20
30
40
50
60
70
80
90
(012) Al2O3
(104) Al2O3
(110) Al2O3
(111)Al
(113) Al2O3
(200)Al
(024) Al2O3
(116) Al2O3
(122) Al2O3
(220)Al
(214) Al2O3
(300) Al2O3
(10(10)) Al2O3
(311)Al
(222)Al
20%
5%
1%

Figure(s)

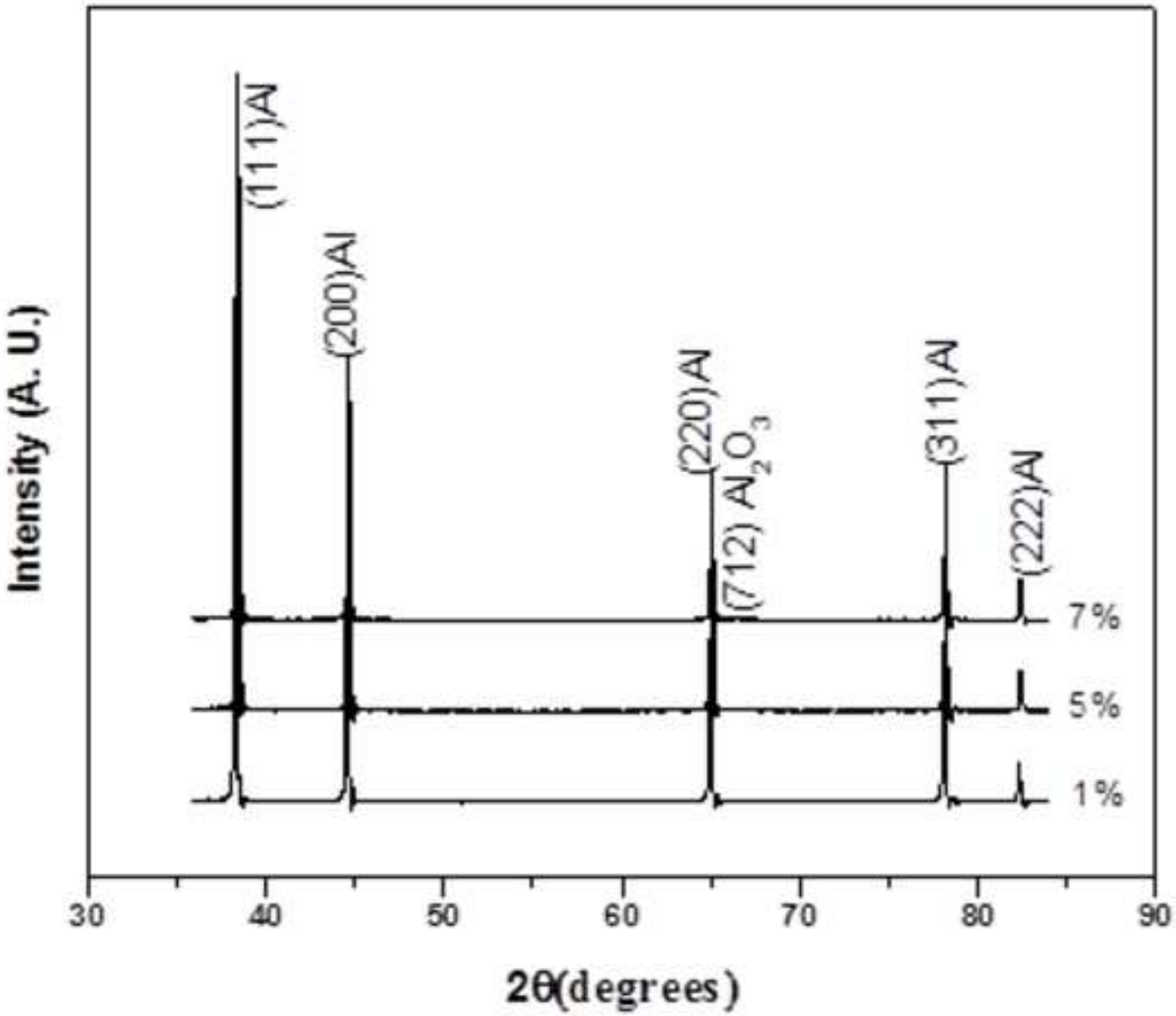
Intensity (A. U.)
(111)Al
(200)Al
(220)Al
(712) Al_2O_3
(311)Al
(222)Al
7%
5%
1%
30
40
50
60
70
80
90
2θ(degrees)

Figure(s)

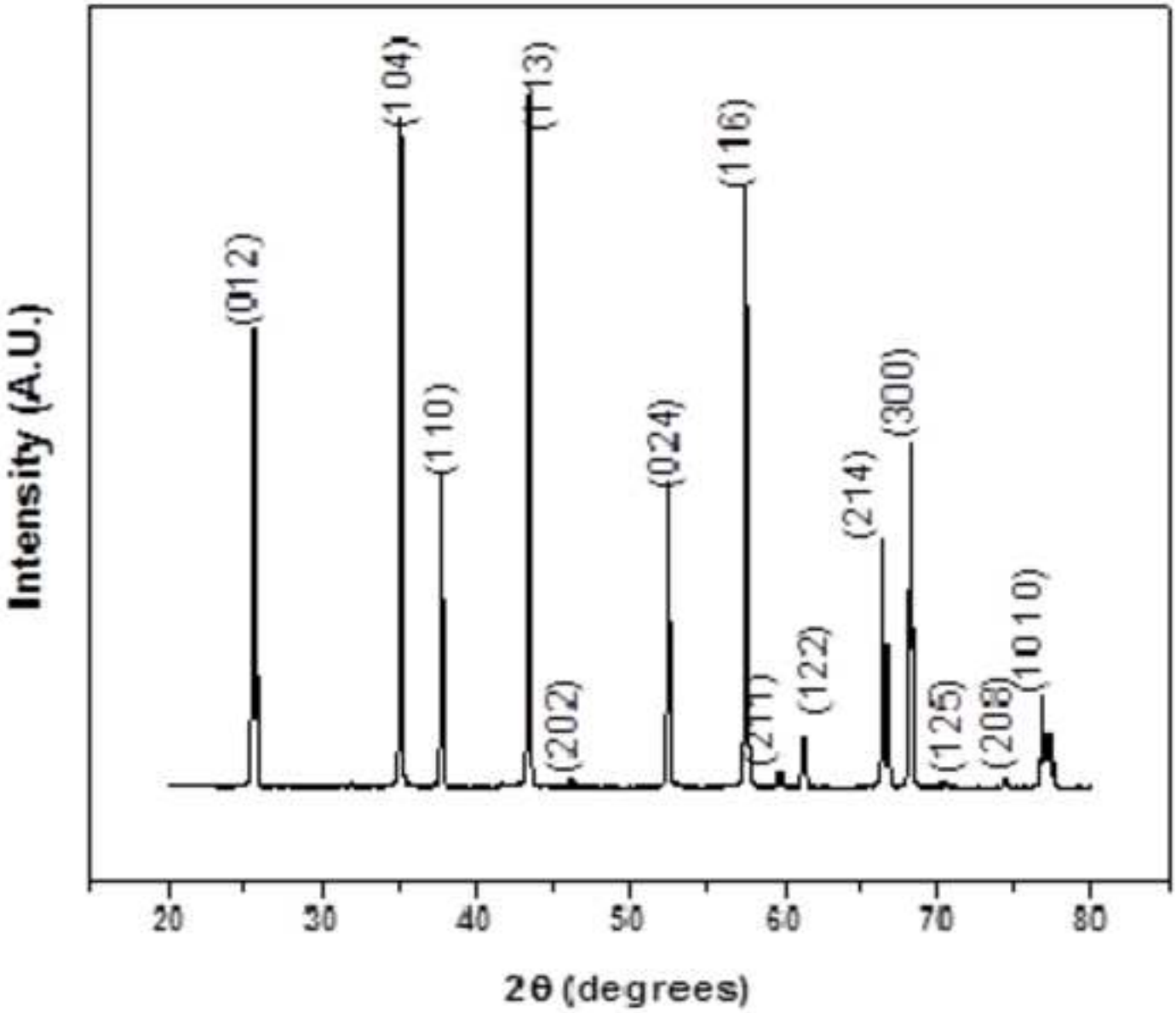
Intensity (A.U.)
(012)
(104)
(110)
(113)
(202)
(024)
(116)
(211)
(122)
(214)
(300)
(125)
(208)
(1010)
20
30
40
50
60
70
80
2θ (degrees)

Figure(s)

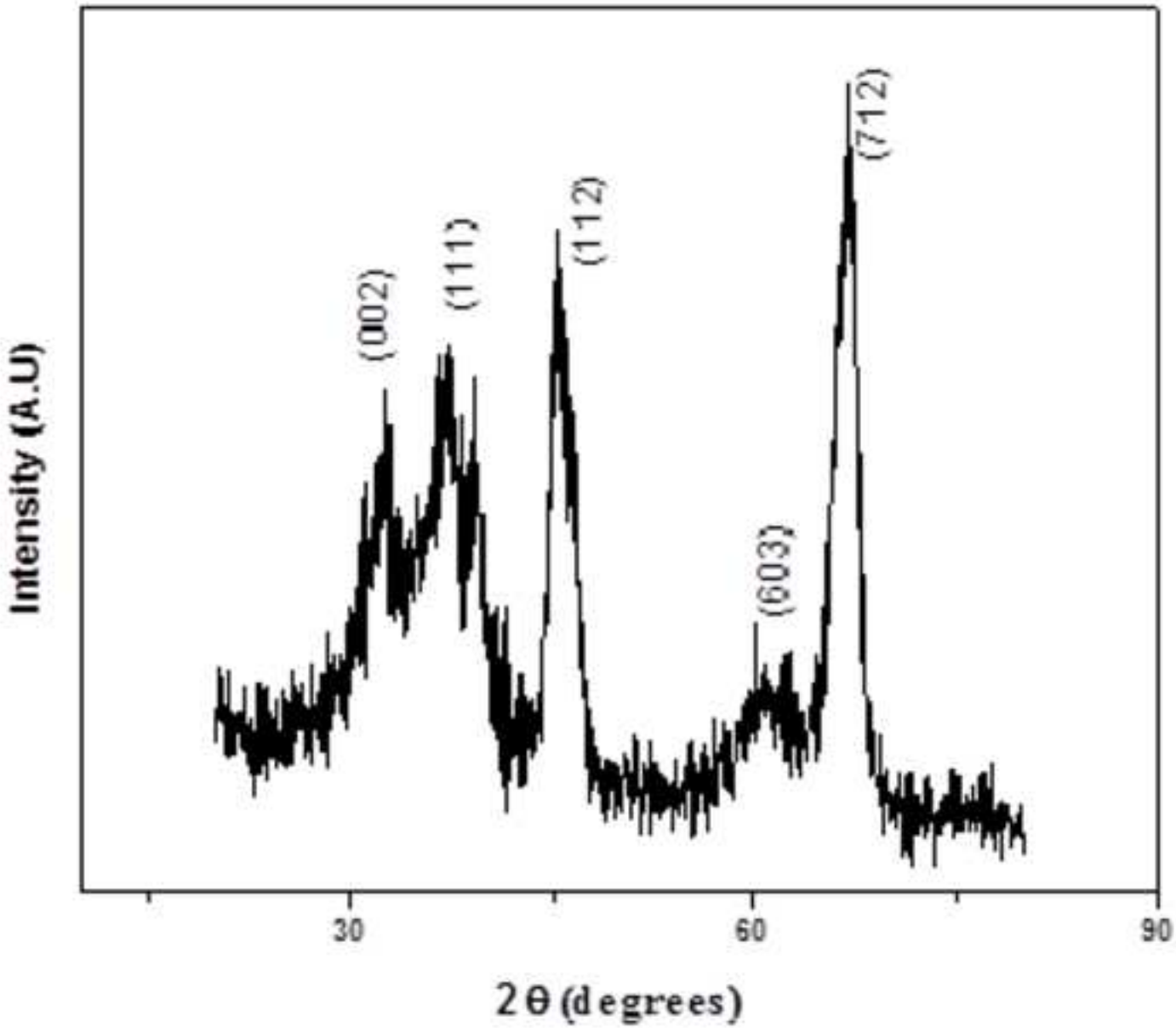

Figure(s)

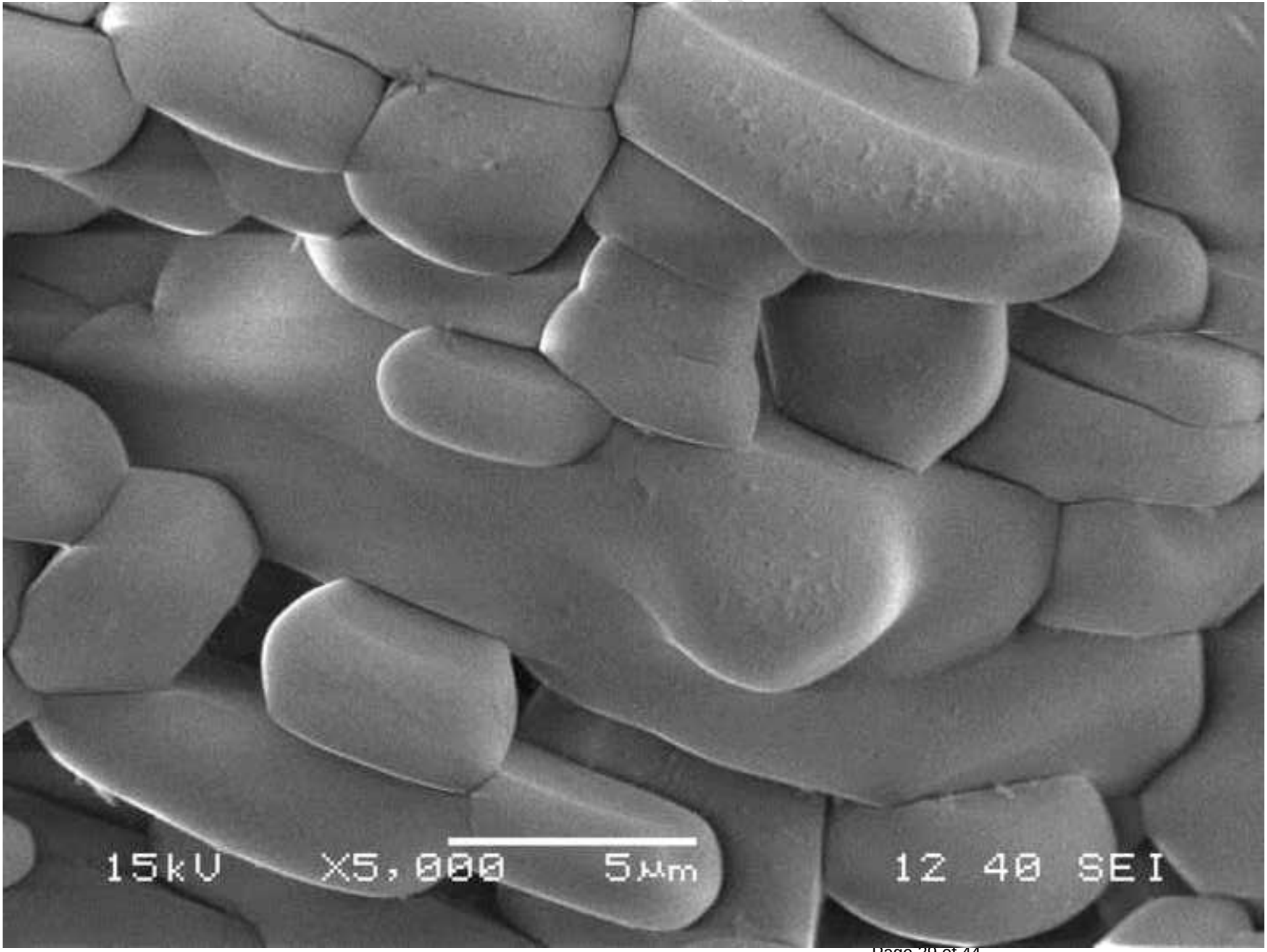

Figure(s)

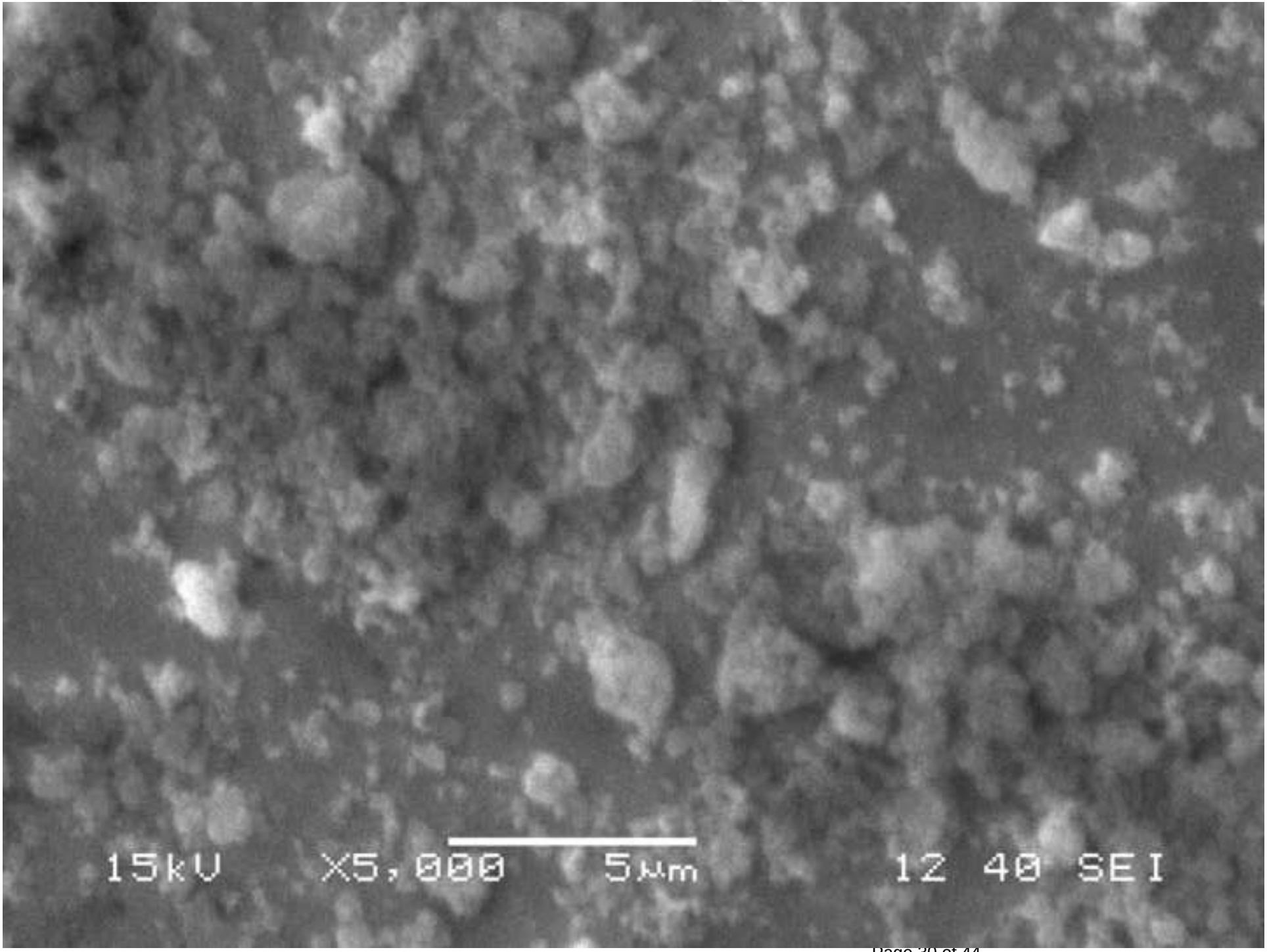

Figure(s)

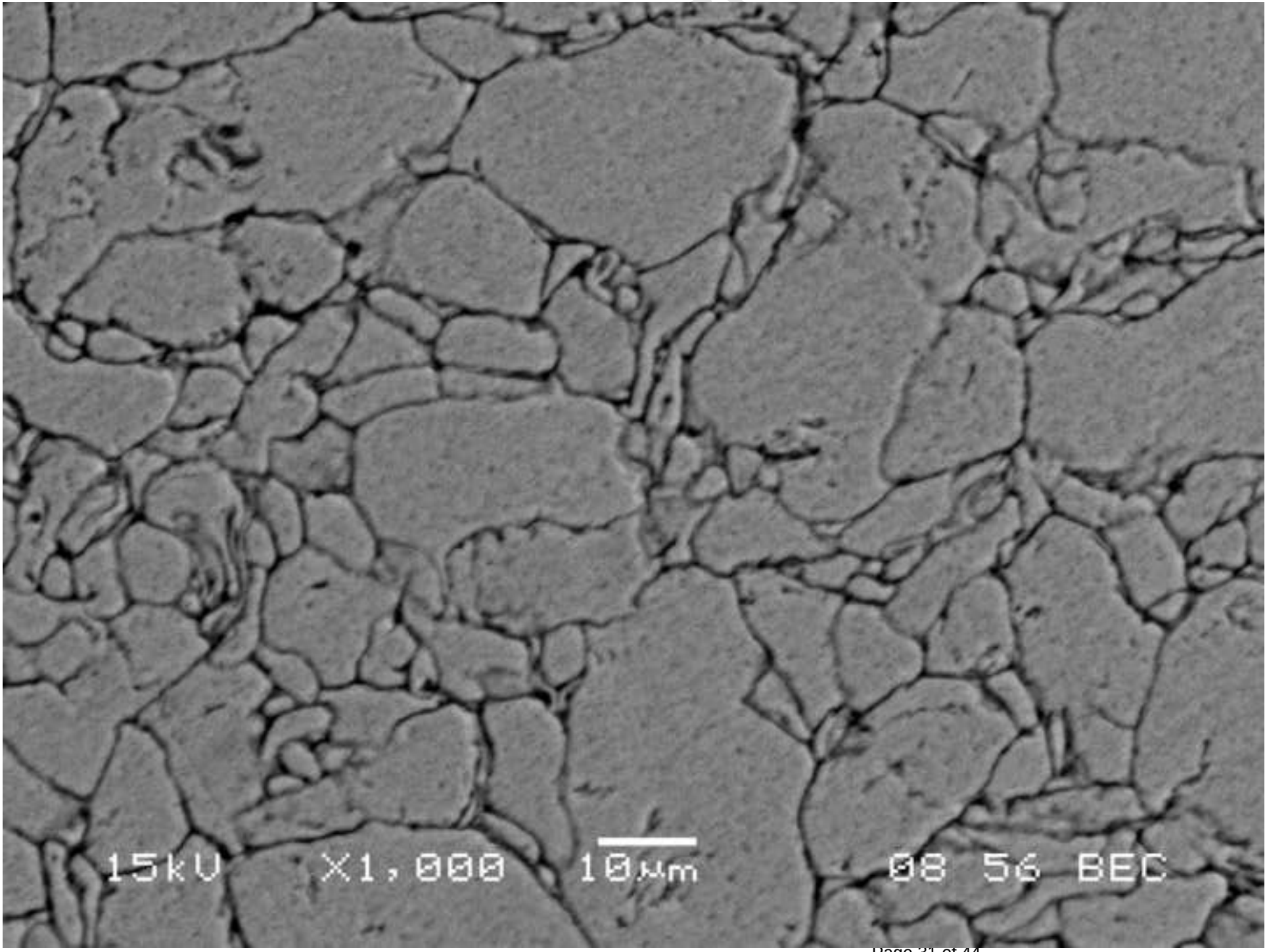

Figure(s)

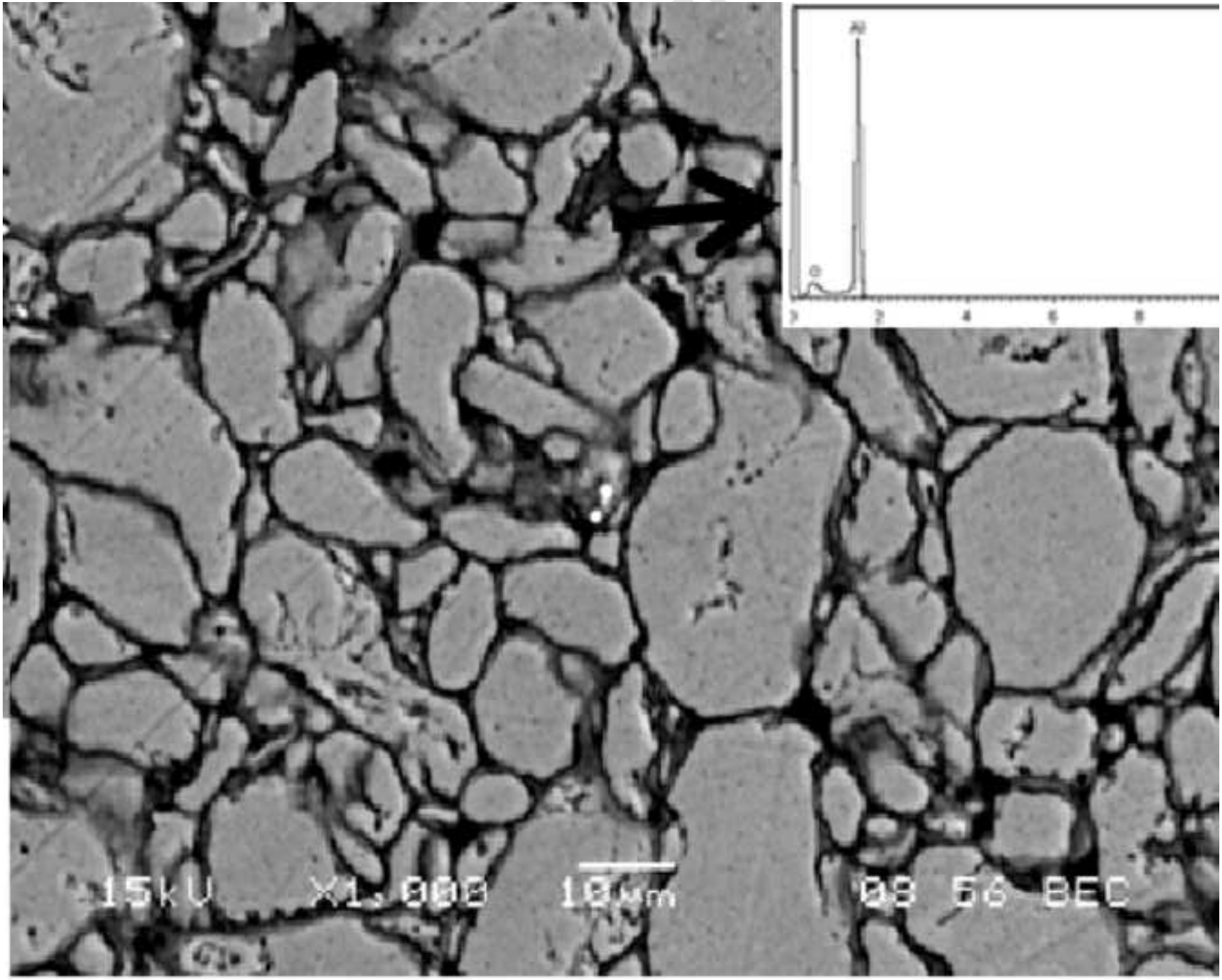

Figure(s)

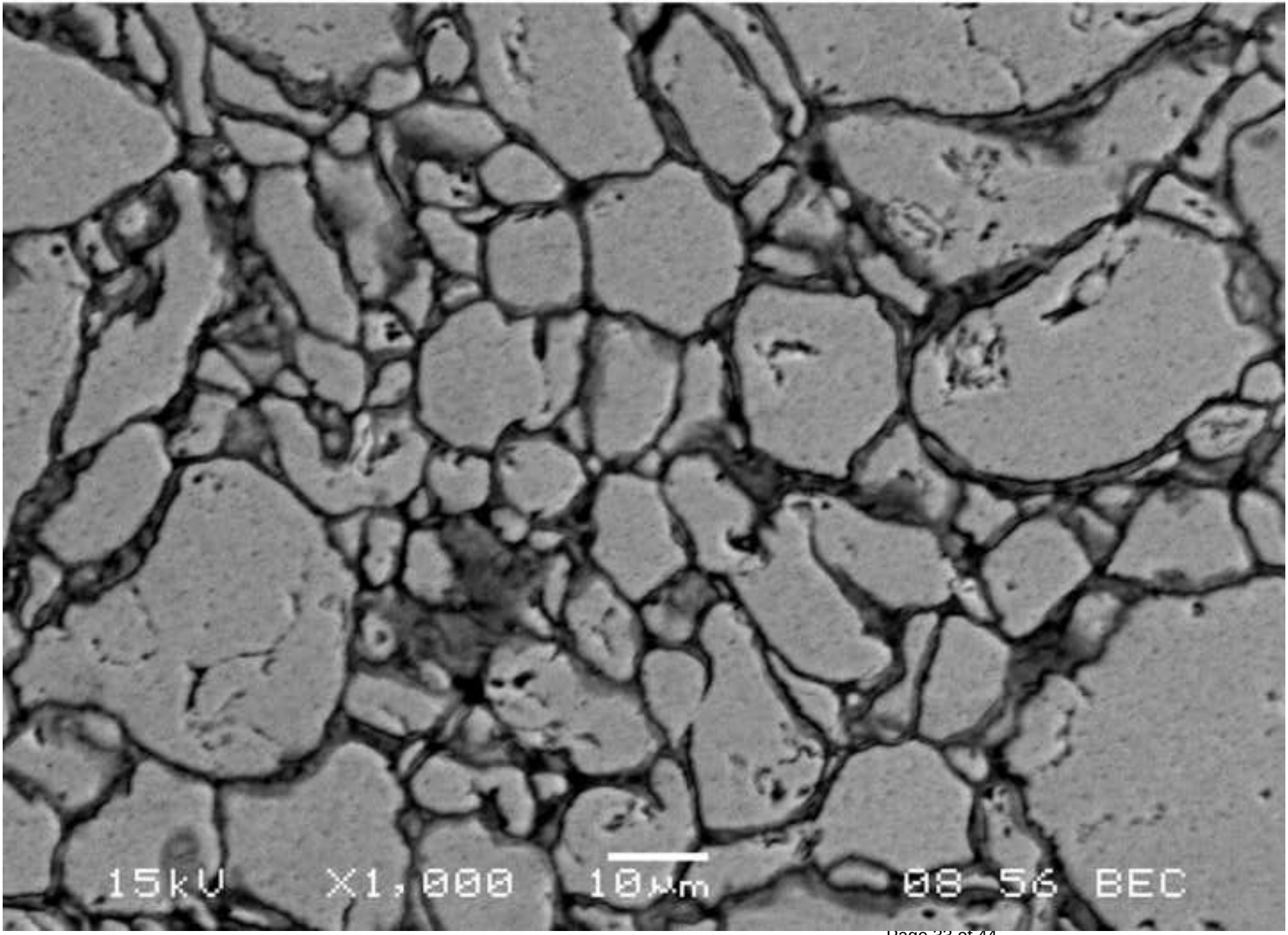

Figure(s)

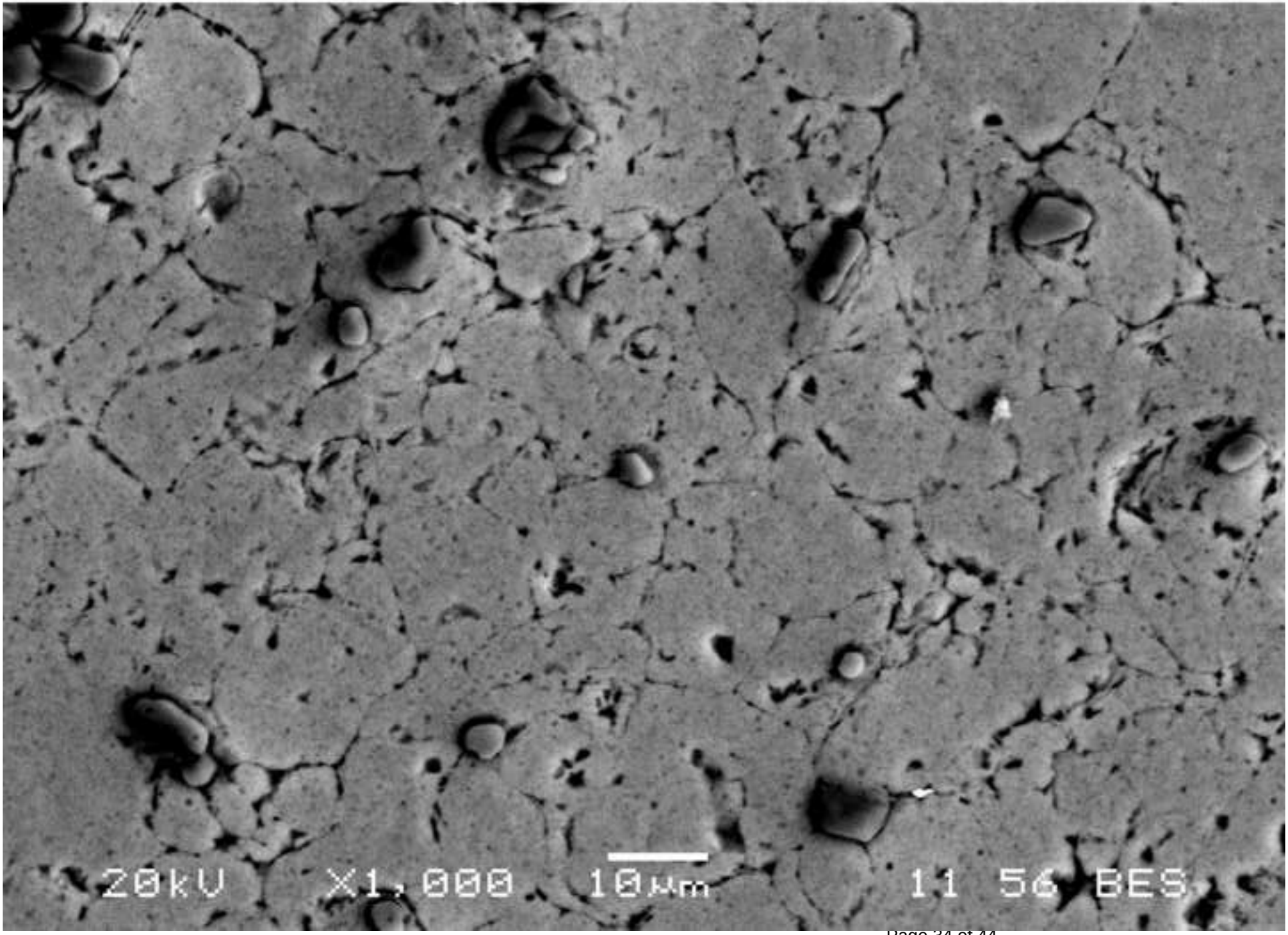

Figure(s)

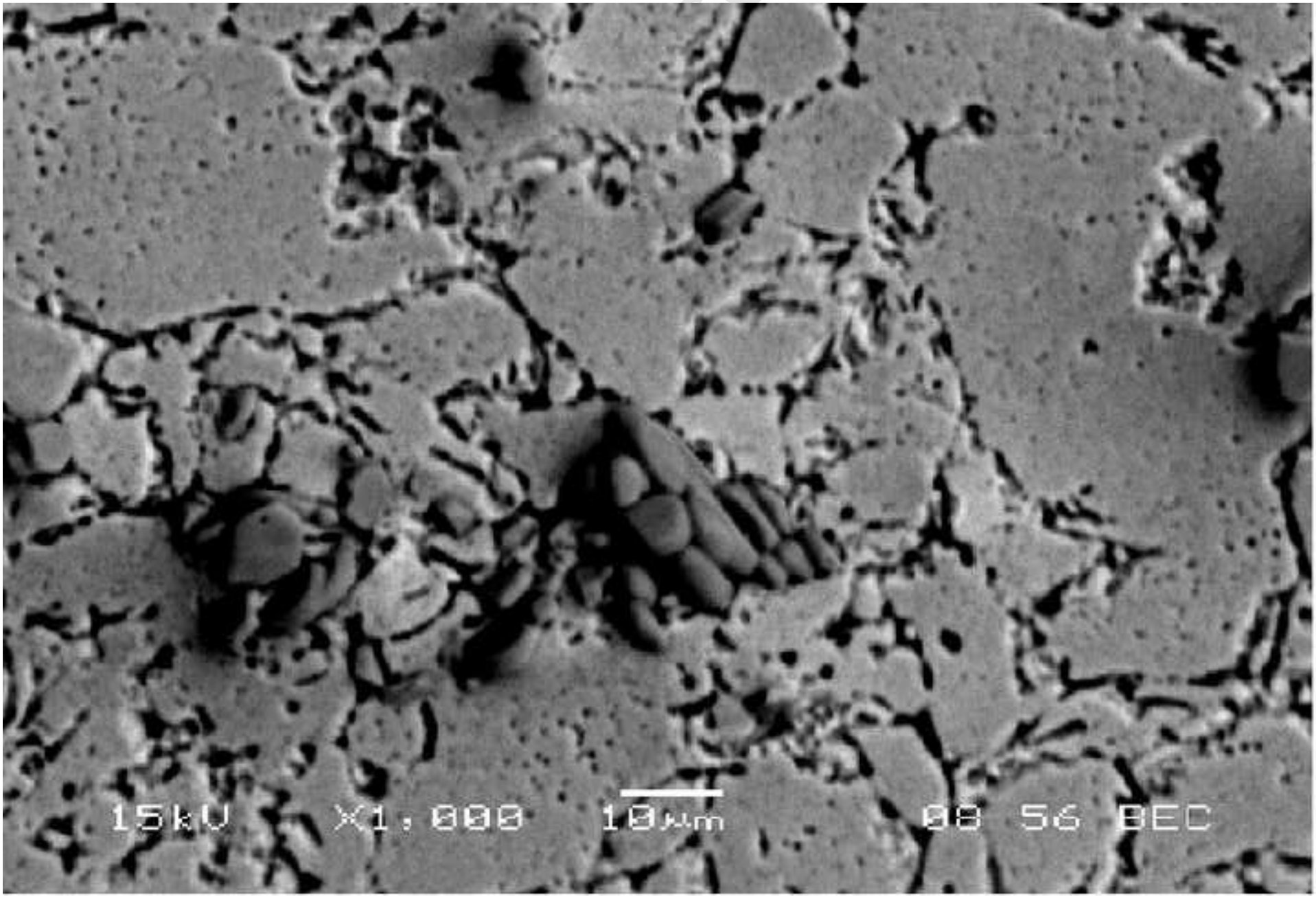

Figure(s)

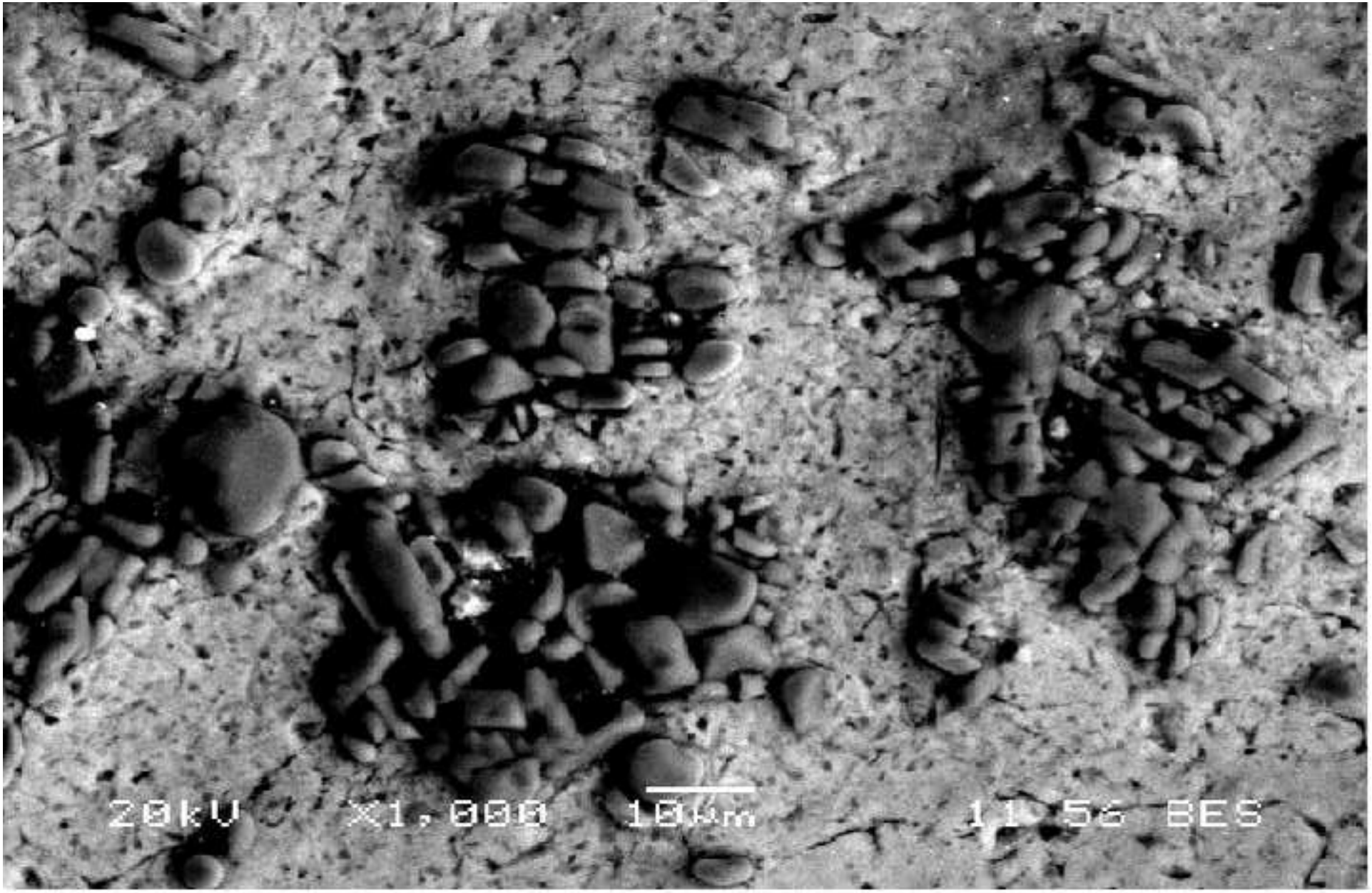

Figure(s)

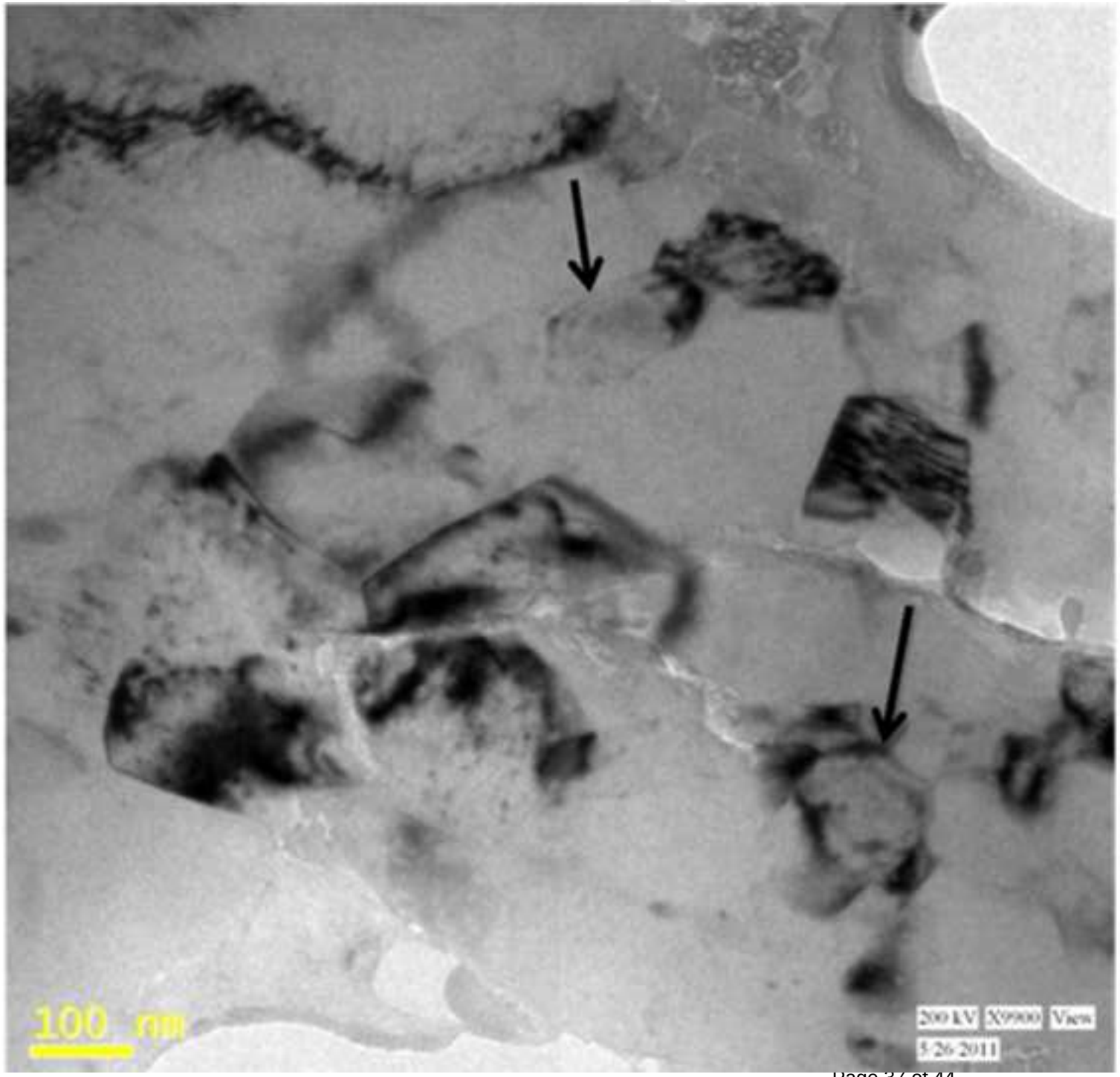

Figure(s)

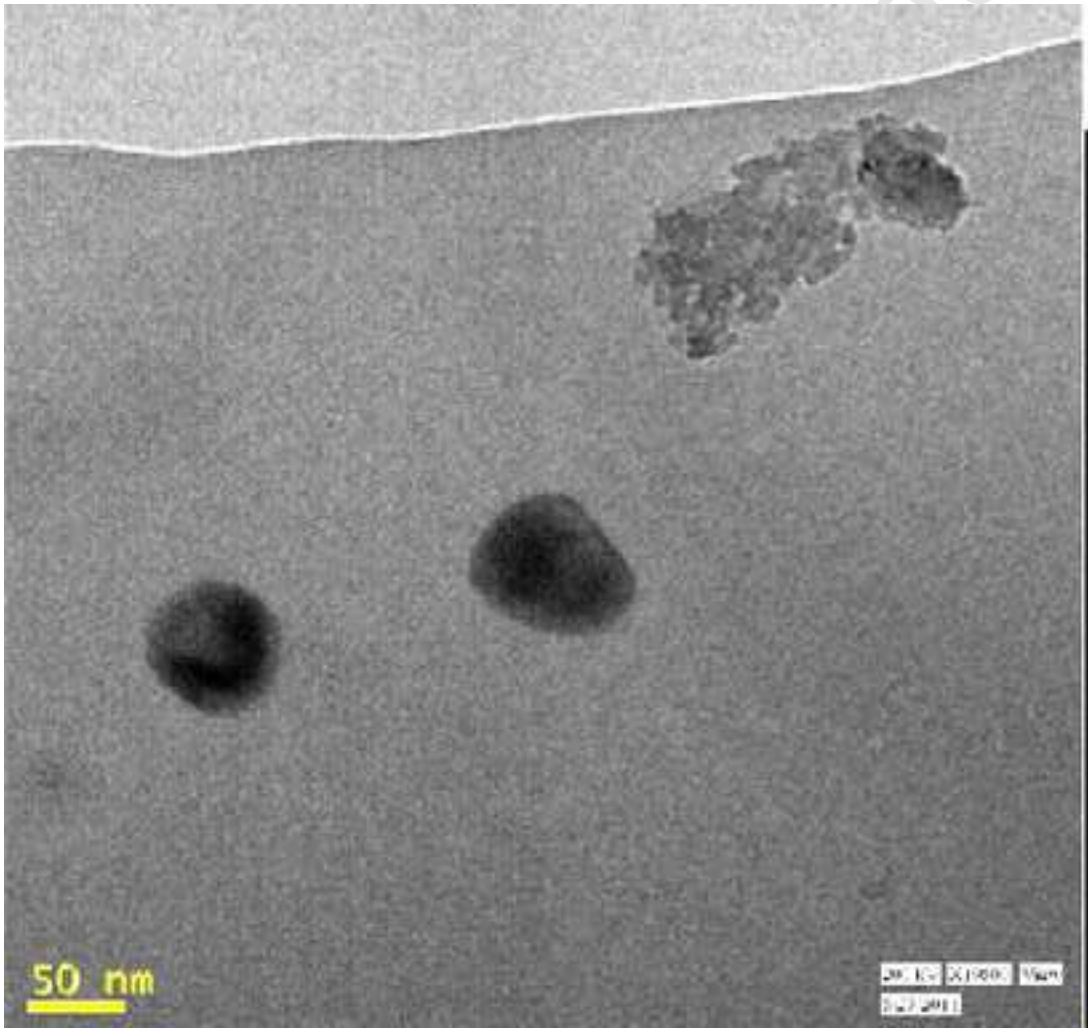

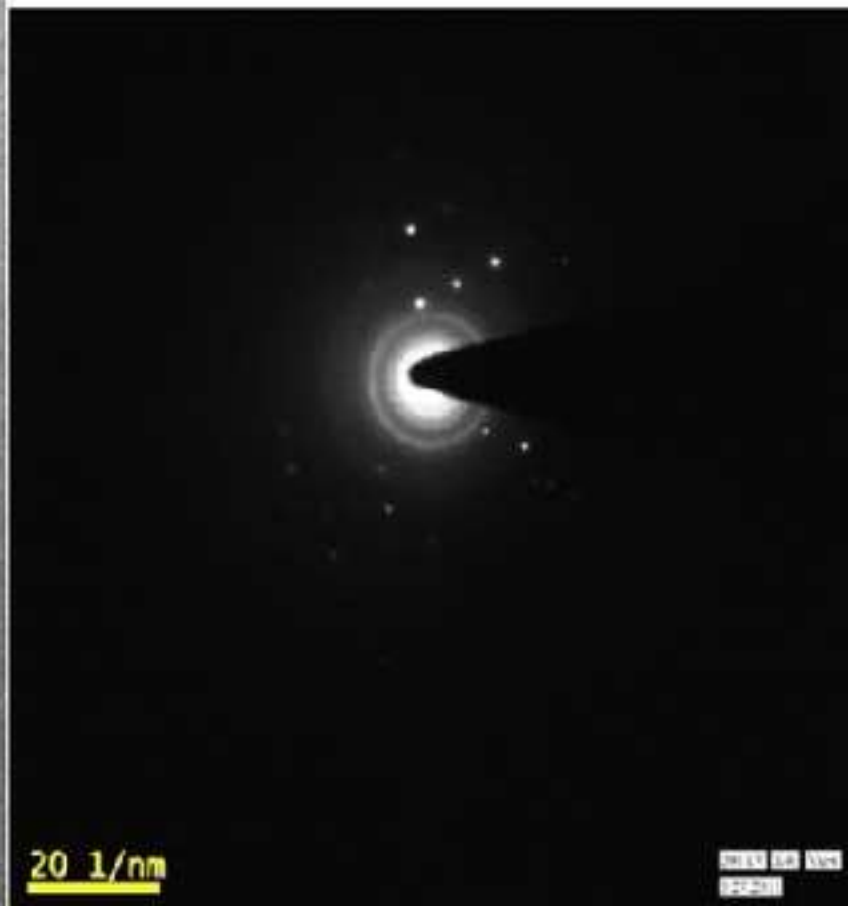

Figure(s)

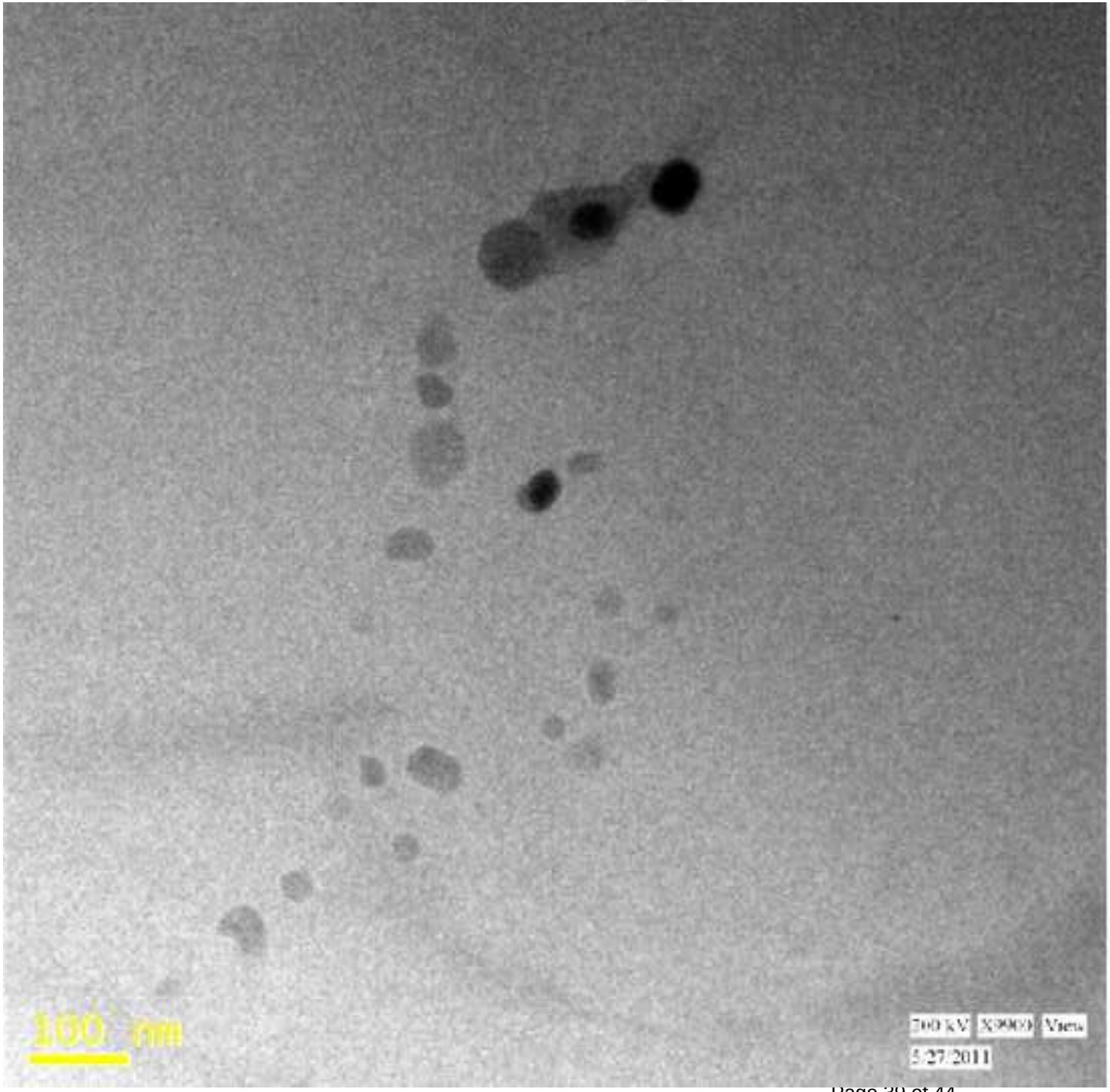

Figure(s)

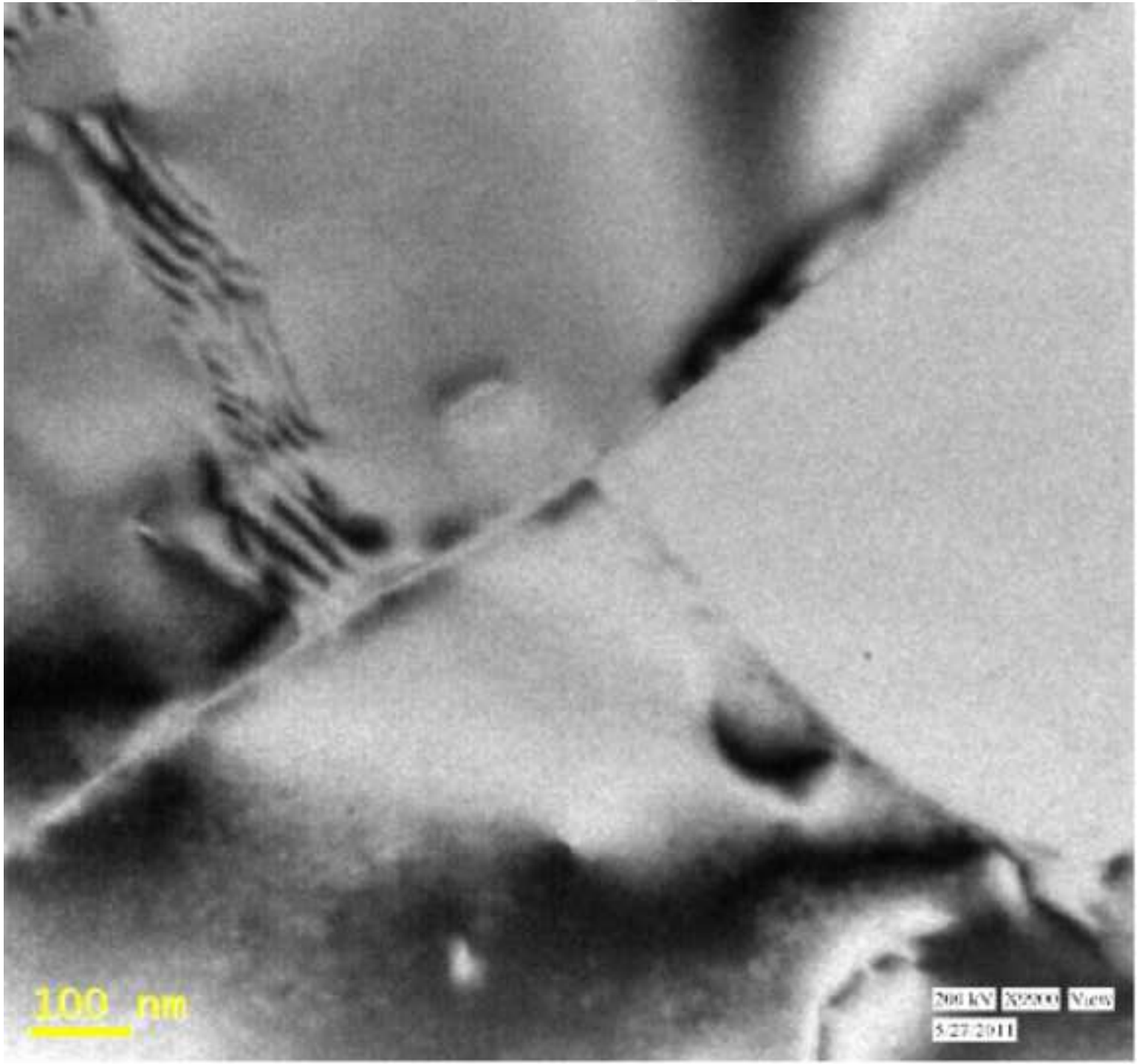

Figure(s)

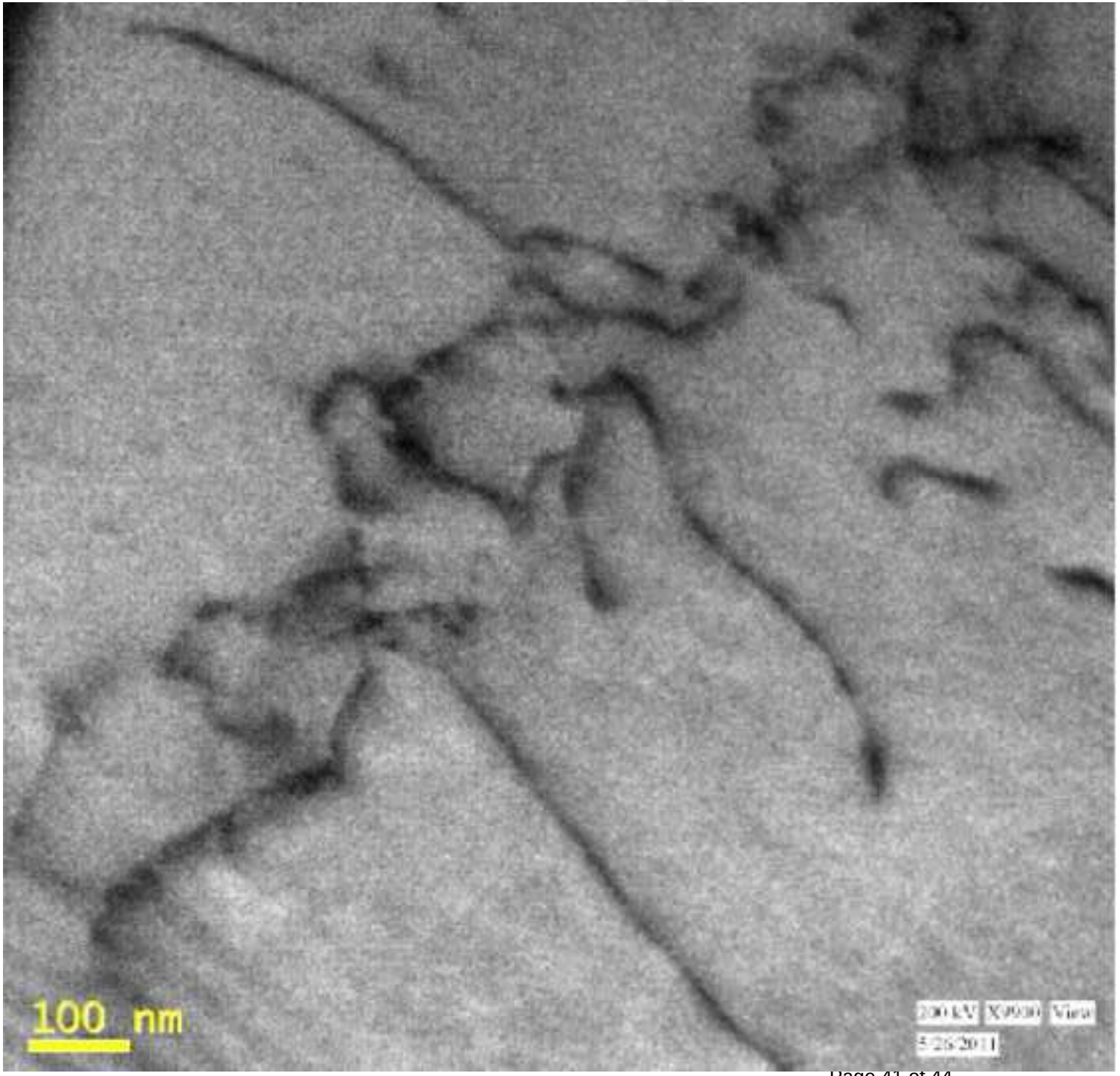

Figure(s)

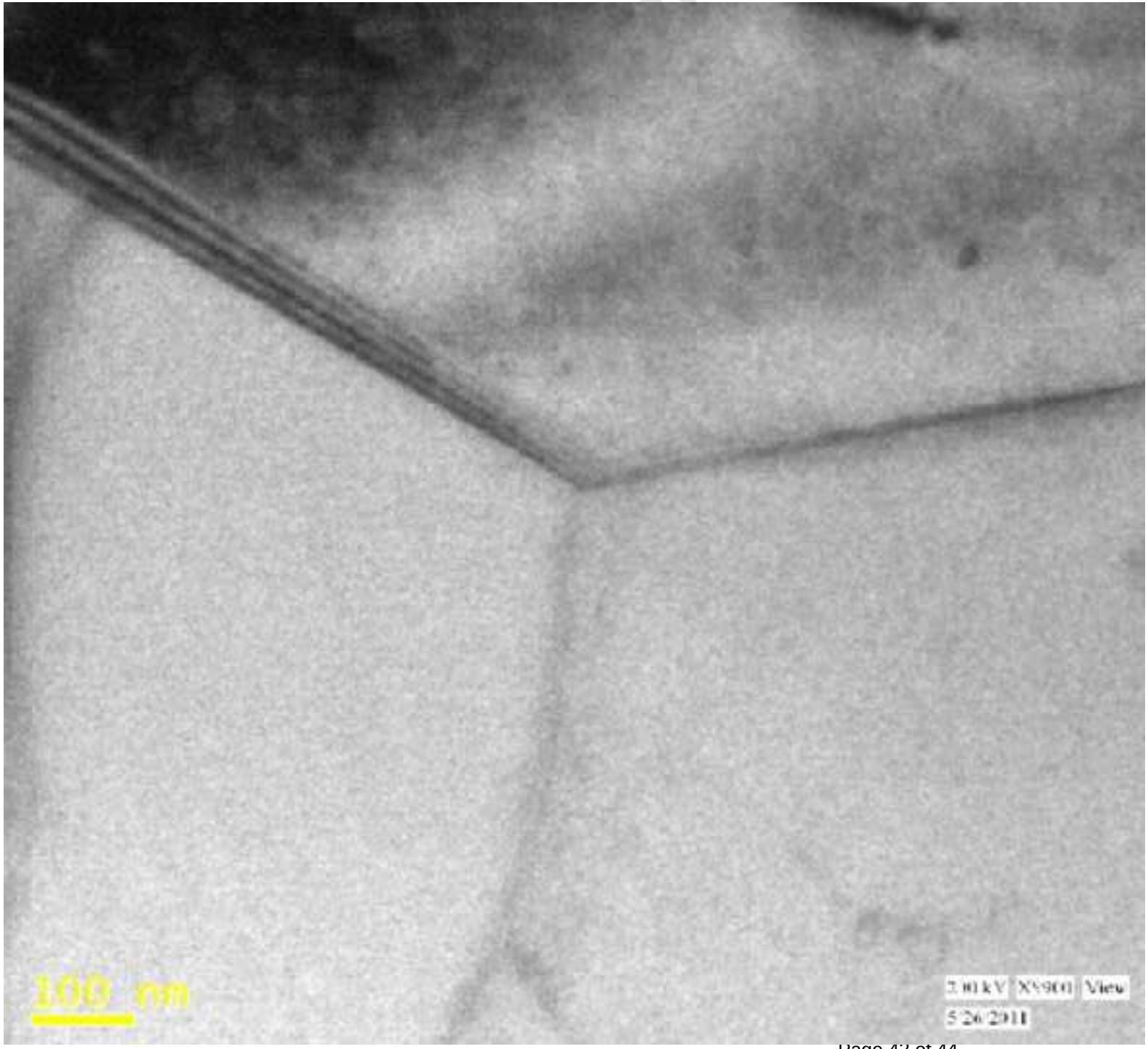

Figure(s)

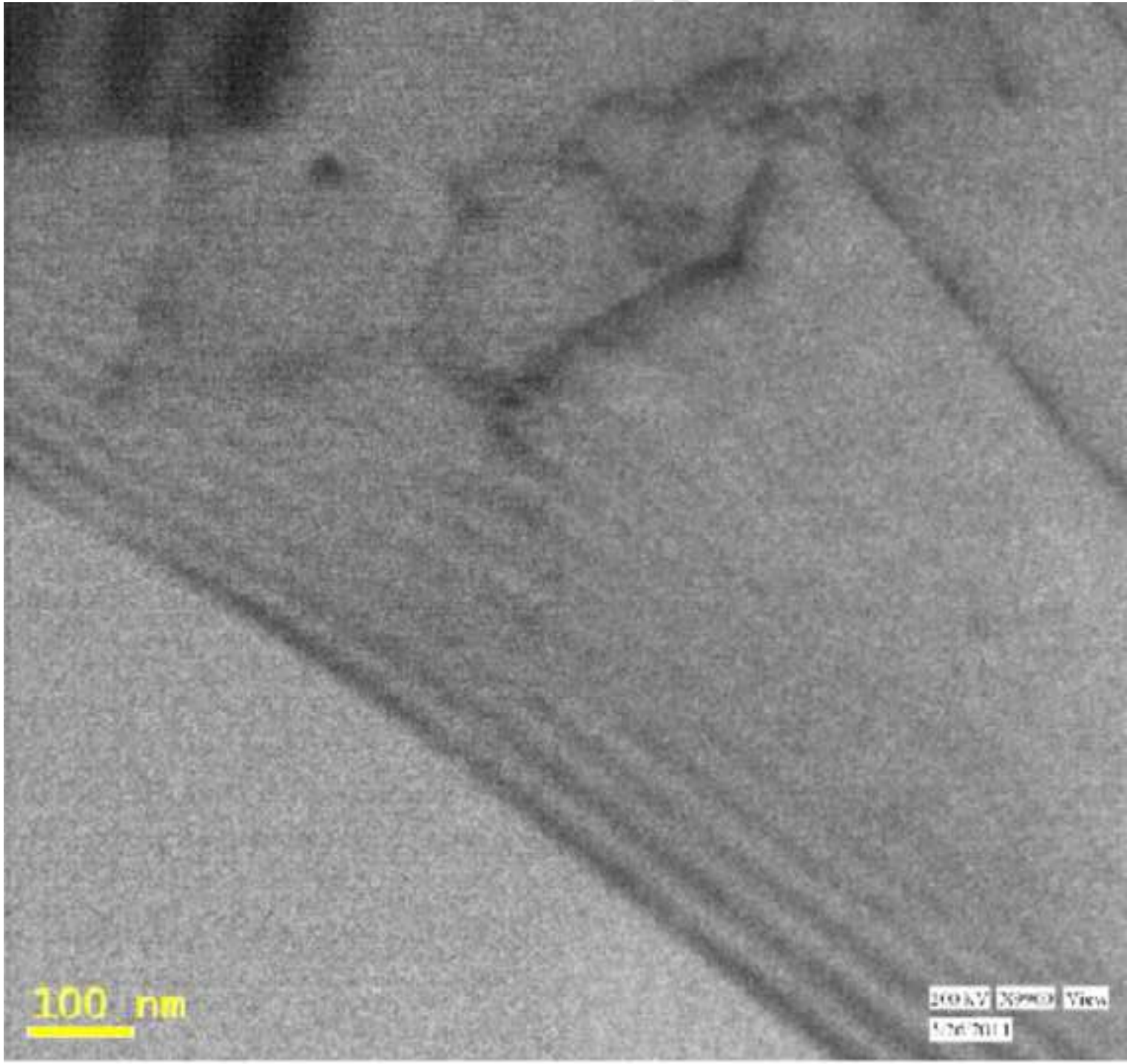

Table 1: Density, microhardness and nanoindentation hardness values of Al-Al_2O_3 micro- and nano-composites

Composition (alumina content in wt. %)	% theoretical density	Microhardness (GPa)	Nanoindentation hardness (GPa)
Nanocomposites			
0.5	95.5	0.36 0.02	
1	99.5	0.32 0.01	0.60 0.07
3	90.1	0.35 0.01	
5	93.6	0.51 0.06	0.49 0.07
7	93.6	0.38 0.03	0.85 0.14
Microcomposites			
1	98.8	0.37 0.01	
5	97.1	0.46 0.04	
20	92.5	0.55 0.02	